Experimental Characterization of Galfenol (FeGa) Alloys

Undergraduate Honors Thesis

Presented in Partial Fulfillment of the Requirements for
Graduation with Distinction at
The Ohio State University

By

Qian Zhang

* * * * *

The Ohio State University

2014

Defense Committee:

Professor Marcelo Dapino, Advisor

Professor Rebecca Dupaix

Approved by

_____

Advisor
Undergraduate Program in
Mechanical Engineering

ABSTRACT

Magnetostrictive materials are a class of smart materials which undergo a change in dimensional shape when subjected to a magnetic field. Galfenol, an alloy of iron and gallium, is a relatively new magnetostrictive material that exhibits favorable magnetostriction combined with mechanical robustness. These characteristics make Galfenol promising in the development of sensors and actuators.

The research characterizes textured polycrystalline Galfenol alloys ($Fe_{81.6}Ga_{18.4}$) under both quasi-static and dynamic conditions, with a focus on understanding the sensing properties of this material. The research provides further improvements to a constitutive model that describes the non-linear piezomagnetic relationships of Galfenol over a range of stresses and applied magnetic fields. In addition, this research aids in the creation of guidelines for analyzing the actuation and sensing behavior of Galfenol, which will allow for improved design of Galfenol-based actuators and sensors.

ACKNOWLEDGMENTS

I would not have been able to complete this research without the help of many individuals. First, I would like to express my gratitude to my advisor, Professor Marcelo Dapino, for giving me the opportunity to work on this project as an undergraduate. I am very grateful for the technical and professional growth I have received under his guidance in the past two years. Next, I would like to thank all my colleagues in the Smart Materials and Structures Laboratory for the friendly discussions throughout my research. I would especially like to thank Zhangxian Deng, Justin Scheidler, John Lason, and Ryan Hahnlen for their help. They were instructional in many aspects of this research and provided technical support when the experiments didn't pan out. I would also like to acknowledge the Department of Mechanical Engineering at The Ohio State University. I express my thanks to Professor Rebecca Dupaix for serving on my committee.

In addition to the people I work with at the Department of Mechanical Engineering, I would like to thank my family and friends. To my friends, Chengcheng Zhang, Jing Liu, Yu Wang, Le Chang, Simon Lee, Mei Han, Jun'ni Bian, Mengjie Li, Yakun Li, Jing Li, Wenjie Song, Jue Wang, Shi Shi, Cathy Kurre, and Mike Kurre, thanks for the support and all the memories. I can accomplish nearly anything without the guidance and support of my parents. Special thanks to my parents for your love, sacrifice, and encouragement.

TABLE OF CONTENTS

LIST OF TABLES

LIST OF FIGURES

CHAPTER 1

INTRODUCTION

1.1 Background

The development of evolving technologies has been linked to changes in the use of materials. Due to their adaptive characteristics, smart materials are attractive for many industry, defense, automotive, biomedical, and aerospace applications.

Smart materials are multi-functional materials that show strong coupling between temperature, applied electric or magnetic field with their mechanical properties. Such coupling provides a built-in mechanism for sensing and actuation. Besides, smart materials have an inherent ability to convert one form of energy to another. The most common smart materials include piezoelectric materials, shape memory alloys, electrostrictive materials, and magnetostrictive materials. Smart material integrated sensors or actuators are useful in applications such as micro- and nanosystems, energy harvesting, and structural health monitoring.

Magnetostrictive materials are a class of smart materials which are promising in the automotive industry and medical devices. Magnetostrictive materials are characterized by the phenomenon of a dimensional change combined with a change in magnetization.

Magnetostrictive materials have two important aspects that are widely being investigated and researched, inverse (actuation) effect and direct (sensing) effect. The inverse effect is a property of magnetostrictive materials that undergo a change in magnetization due to the applied stress, and the direct effect is that of a change in dimensions in the direction of the applied magnetic field. The inverse and direct magnetostrictive effects are applicable to measure and control the responses in an actuating or sensing system [1]. The actuation characteristics allow magnetostrictive materials to be used in developments of sonar transducers and vibration control. Making use of the sensing characteristics could aid in designs of force torque sensors and acoustic sensors [2].

The history of magnetostrictive materials began in 1842 by English physicist James Joule. He discovered that a sample of iron changed its length when subjected to a magnetic field. This discovery led to the development of implementing magnetostrictive materials in actuation and sensing devices. Examples of common magnetostrictive materials are iron, cobalt, and nickel. These materials were first used in telephone receivers, hydrophones, torque-meters, and scanning sonar [3]. Although iron, cobalt and nickel have robust mechanical properties with tensile strengths more than 250 MPa, these materials have small magnetostrictive strain capabilities [4]. In the early 1960's, researchers discovered that certain rare earth elements, such as terbium (Tb) and dysprosium (Dy), show giant magnetostriction effects, on the order of 10,000 microstrain. However, since the rare earth elements have low Curie temperatures, large magnetostrictions can be observed only at cryogenic temperatures. In the 1970s, large magnetostrictions on the order of 0.2% were available at room temperature by adding the magnetic transition metals, such as iron and

nickel, to the highly magnetostritive rare earth elements. Terfenol, an alloy of iron and terbium, was originally developed at the Naval Ordinance Laboratory. The addition of dysprosium to Terfenol was found to lower the drive amplitude of the magnetic field [5]. These alloys known as Terfenol-D (an acronym from **ter**bium iron(**fe**) **N**aval **O**rdinance **L**aboratory - **D**ysprosium), which exhibits a saturation magnetostriction up to $1600 * 10^{-6}$ when subjected to a magnetic field of 160 kA/m [6]. Terfenol-D is of high interest because of its large magnetostriction. However, scientists found that Terfenol-D is sensitive to fluctuation in temperature, and its brittle nature limits its applications in harsh or shock-prone environments. This issue stimulated researchers and scientists to synthesize a new magnetostrictive material that has superior mechanical properties. In 1999, a new magnetostrictive material, Galfenol (an acronym from **gal**lium iron (**fe**) **N**aval **O**rdinance **L**aboratory), an alloy of gallium and iron, was invented by the Magnetic Materials Group at Naval Surface Warfare Center, Carderock Division (NSWCCD).

Galfenol is a mechanically robust magnetostritive material, which is of increasing interest as it can be integrated into actuators, sensors, and energy harvesting devices. They have desirable properties including favorable magnetostrictive strains at a low saturating magnetic field as well as steel-like mechanical strength. These unique metallurgical properties allow Galfenol alloys to accommodate bending, tensile, and compressive loading. Also, Galfenol can be easily shaped utilizing conventional machining techniques, rolled, welded, and forged while maintaining its magnetic performance. Compared to Terfenol-D, Galfenol has smaller hysteresis and lower coercivity. This means that Galfenol is easier to magnetize and has less loss during operation. Moreover, Galfenol has a significantly higher

Curie temperature than Terfenol-D, so Galfenol based devices can function within a large temperature range [7].

Galfenol alloys textured by different manufacturing processes would result in different magnetostrictive and mechanical performances. Besides, the amount of gallium in the Galfenol alloy would also affect its mechanical properties. This research has focused on the textured polycrystalline 18.4 at.% Ga Galfenol alloys for two reasons. First, the polycrystalline forms have potentially higher production yields and superior mechanical properties over those of single crystals. Secondly, recent research shows that around 18% Ga Galfenol alloys exhibit a higher magnetostriction [8].

To better utilize Galfenol in industry, constitutive relations need to be derived for characterizing the material behavior. Characterization is essential for predicting Galfenol's response to increase the reliability and performance. In this research, characterization of Galfenol at various magnetic fields, stresses, and frequencies were studied and analyzed. This research will improve an existing multi-physics Galfenol model, which will allow for more accurate designs of actuators and sensors, and make Galfenol based sensors be more competitive with established sensor technologies, such as piezoelectric sensors. Since Galfenol is a relatively new magnetostritive material, more work needs to be conducted to better understand its behavior.

1.2 Literature Review

1.2.1 Magnetostrictive Fundamentals

Magnetostrictive materials have a structure such that the magnetization divides itself into localized volumes known as magnetic domains, where the magnetic dipole moments are aligned parallel to one another [9]. Due to this structure, there exists a coupling of the magnetic and mechanical states of these materials. When a magnetic field is applied, the magnetic domains rotate along the direction of the field. The rotation and re-orientation of the magnetic domains cause internal strain in the material structure. This dimensional change of these materials under the influence of an external magnetic field is known as magnetostriction, and magnetic dipole moment per unit volume is called magnetization [10]. The magnetostrictive effect can be seen more clearly in Figure 1.1. Two important aspects of magnetostrictive materials are actuating and sensing effect. The following schematic images, Figure 1.2 and Figure 1.3, show inverse and direct magneostrictive effect, respectively. In these figures, ellipse stands for magnetic domain, and arrow indicates magnetic dipole moment.

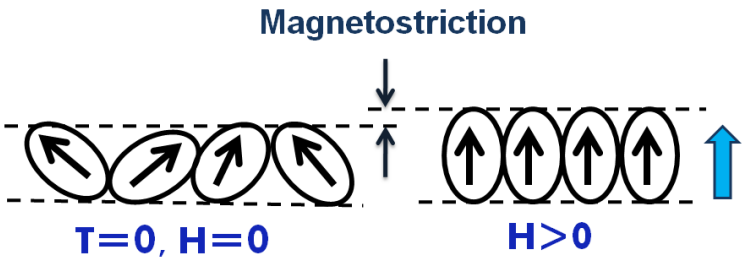

Figure 1.1: Orientation of magnetic domains caused by external fields

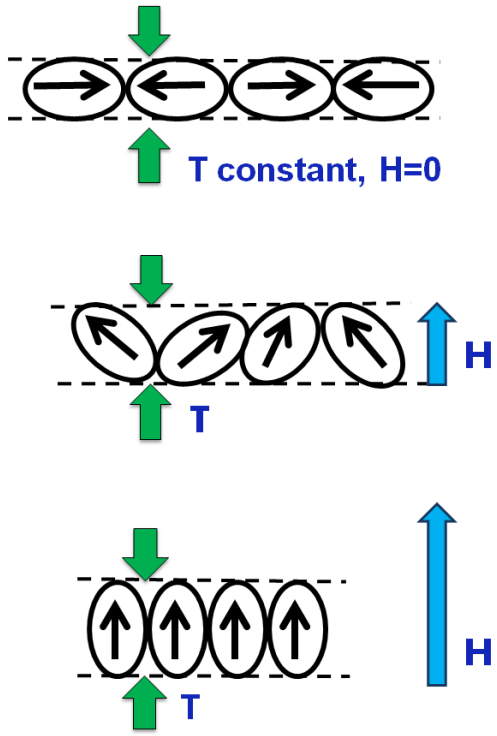

Figure 1.2: Schematic of inverse magneostrictive effect (Actuation)

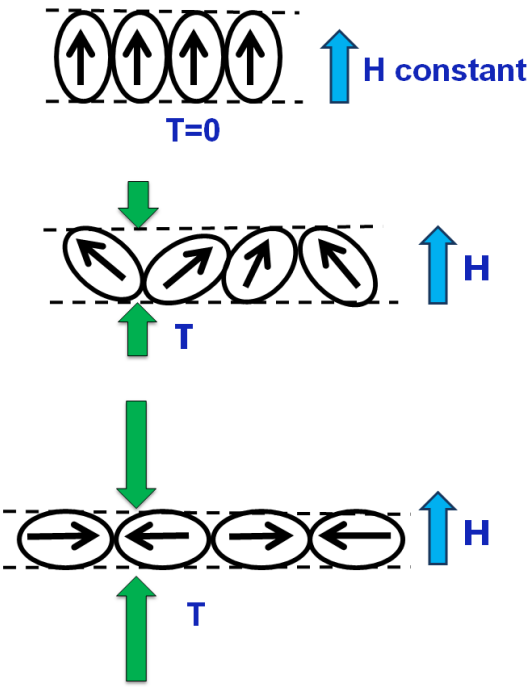

Figure 1.3: Schematic of direct magnetostrictive effect (Sensing)

The response of magnetization M, or flux density $B = \mu_o (H + M)$, and strain S to a change in stress T and magnetic field H is a non-linear. The response also depends on material history. The nonlinearities arise from two major components, saturation and anisotropy. As the applied field increases, domains within the material will align themselves with the external field. The magnetism curve becomes flat when all the magnetic domains align with the applied field, known as magnetic saturation. The saturation phenomenon can be observed in both magnetization and magnetostriction. Magnetostrictive materials are directionally dependent, known as anisotropy, and have preferred crystallographic directions. The magnetic anisotropy in these materials is defined as the tendency of a magnetic moment to point in a particular crystalline direction because of the electrical attraction or repulsion between its attached electronic charge cloud and the neighboring charged ions [11].

To account for the nonlinear behavior, the coupled linear piezomagnetic equations were developed and modeled by,

$$S_{ij} = [s^{H}_{ijkl}]T_{kl} + [d_{ijk}]H_k \tag{1.1}$$

$$B_{ij} = [d_{ijkl}]^{*}T_{kl} + [\mu^{T}_{ijk}]H_k \tag{1.2}$$

These equations use the following coupling coefficients: magnetic flux density vector B_{ij}, magnetic field vector H_k, stress tensor T_{kl}, strain tensor S_{kl}, $[d]$ is the piezomagnetic constant matrix, $[s^{H}_{ijkl}]$ is the compliance coefficient matrix, and $[\mu^{T}_{ijk}]$ is the material permeability matrix. Equation (1.2) is mostly researched for implementing magnetostrictive materials in energy-harvesting applications. This is due to the

phenomenon that changes in stress would cause changes in magnetic flux density, which can be used to harvest vibrational energy [7].

1.2.2 Static Galfenol

The amount of gallium in Galfenol alloys has a significant effect on the magnetostrictive performance. The effect of the composition of Galfenol was first described in 2003 [12]. Recently, a study has updated this effect regarding how the amount of gallium of Galfenol affects the material properties, as shown in Figure 1.4.

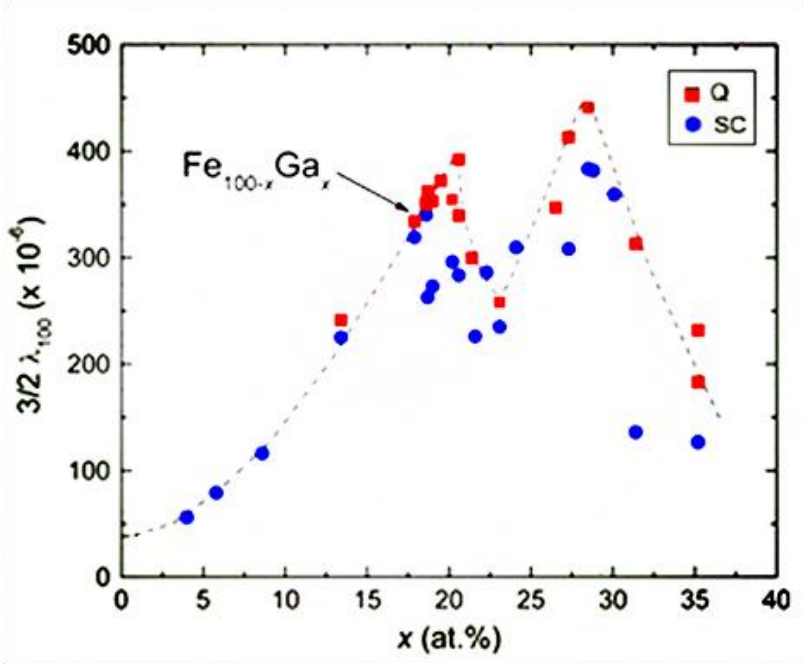

Figure 1.4: Dependence of magnetostriction on Ga content [13]

In Figure 1.4, Q indicates the Galfenol sample was water quenched from 1000 °C, SC means the sample was slow-cooled at 10 °C/min from 1000 °C. The figure shows that

Galfenol alloys has a peak in magnetostriction with a composition of ~20.5 at% gallium for water quenched and ~17 at % gallium for slow-cooled. The second peak in magnetostriction appears at ~ 27.5 at % gallium, and in between these two compositions, a low in magnetostriction is observed at 23.5 at % gallium. For this reason, Galfenol alloys with the composition near the peak have been identified as a region of interest. In this research, a Galfenol sample with 18.4 % gallium was used and characterized.

1.2.3 Quasi-Static Characterization

Kellogg and Flatau [4, 14] have shown the temperature effect on the magnetostriction and magnetization of Galfenol. The results showed that under a condition of an 800 Oe applied field and 45.3 MPa stress, the maximum magnetostriction declines 12% from 340×10^{-6} at $-21\,^{o}\mathrm{C}$ to 298×10^{-6} at $80\,^{o}\mathrm{C}$. Similarly, the maximum magnetization declines 3% from 1313 kA/m to 1265 kA/m. In this research, the characterization was conducted at room temperature.

Previous work on the quasi-static characterization of textured polycrystalline 18.4 at% gallium Galfenol alloys (the same Galfenol sample used in this research) were tested by Mahadevan [20]. However, the results show inconsistencies as the data points from the sensing measurements do not always match the field-magnetization curves. Thus, the same Galfenol sample was used in this research for a more accurate characterization. A constitutive model was developed by Evans and Dapino [15] for simulating the constitutive behavior of Galfenol. This model relates magnetization and strain to magnetic field and

stress, which greatly improves the efficiency and accuracy of analyzing the magnetostrictive behavior of Galfenol.

1.2.4 Dynamic Characterization

Dynamic characterization is of interest because actuators or sensors are often used over a wide range of frequencies. Studies on how the input frequencies affect the output would allow for more accurate designs of Galfenol based devices. Previous work was completed by Poeppelman [16] for the actuation measurements under dynamic conditions. The variation in magnetization and strain at various input frequencies was determined and analyzed. The sensing measurements at various input frequencies were conducted by Walker [25]. However, only stress-magnetization curves were tested, and not enough measurements were conducted (at five different frequencies: 10 Hz, 50 Hz, 100 Hz, 500 Hz, 1000 Hz). Therefore, to further improve the Galfenol model, this research characterized the Galfenol sample at dynamic conditions with a comprehensive set of input frequencies. Moreover, stress-strain curves were also characterized to obtain a better understanding of how strain changes at different input frequencies.

1.3 Project Objective

In this research, a textured polycrystalline 18.4 at.% gallium <100> oriented research grade Galfenol sample was characterized. The first objective of this research is to advance

the characterization of Galfenol under quasi-static conditions. Both actuation and sensing measurements were conducted through major loop testing, and the sensing measurements involved an additional study of minor loop responses. The measurement apparatus was modified based on a previous design [16, 25]. Appropriate sensors and data acquisition were utilized to gather data and record the observed response.

The second objective is to focus on the sensing characteristics of the Galfenol sample under dynamic conditions. Thus, the relationship of magnetization versus stress curves as well as strain versus stress at various frequencies was of interest. This characterization looked at how the output varied with different input frequencies. The tests were conducted with a smaller step of input frequency. To fully understand these responses, sensitivity, hysteresis loss, and elastic of modulus were also analyzed and discussed. The final aspect of this research was to utilize these experimental results to reconcile a majority of the differences between experimental results and simulated responses for updating design parameters and further optimize the Galfenol model.

CHAPTER 2

QUASI-STATIC CHARACTERIZATION

Quasi-static characterization provides an understanding of the nonlinear and hysteretic behavior of Galfenol without the effects of system dynamics. The characterization was conducted under quasi-static conditions through both actuation and sensing measurements. The actuation measurements were conducted by applying a sinusoidal field under different constant stresses. The sensing measurements were completed by applying a sinusoidal stress under different constant magnetic fields. The actuation characteristics were studied based on two relationships, magnetization (or flux density) versus field, and strain versus field. Similarly, the sensing characteristics were analyzed from the relationship of magnetization (or flux density) versus stress, as well as strain versus stress.

2.1 Galfenol Sample Description

In this research, a highly textured, <100> oriented polycrystalline 18.4 at.% gallium Galfenol sample was used for characterizations. The Galfenol sample is shown in Figure 2.1 [16]. The Galfenol sample was purchased from Etrema Products, which has a

cylindrical shape with 6.35 mm (0.25 in.) in diameter and 73.66 mm (2.9 in.) in length. The ends of the Galfenol rod were threaded with a size of ¼ x 28 using standard HSS tools and thread cutting procedures. The length of the threaded portion is 13.3 mm (0.525 in.). The purpose of the threaded ends was for the Galfenol rod to couple with the standard rod of the load frame, as well as to connect the aluminum end cap which adapted to the base of the load frame.

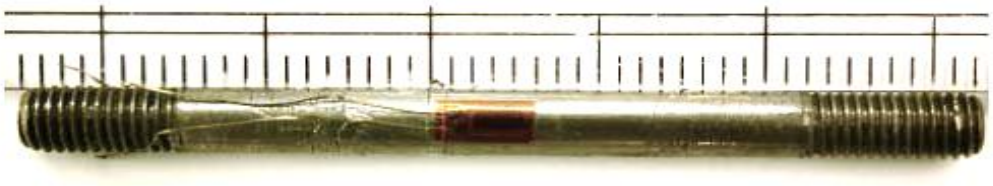

Figure 2.1: Textured polycrystalline Galfenol ($Fe_{81.6}Ga_{18.4}$) from Etrema Products [16]

2.2 Magnetic Circuit

The magnetic circuit is a major component in the characterization of Galfenol, which provides control of the magnetic domains in the Galfenol sample. The magnetic circuit used in this research was designed and constructed by Poeppelman [16]. This circuit consists of two drive coils and two steel laminates, as shown in Figure 2.2. When a current is applied to each coil, a uniform magnetic flux would be produced and flow through the Galfenol sample in the axial direction. Two excitation coils were used to double the amount of magnetic flux. The magnetic field generated on the surface of the Galfeol

sample can be calculated from the input current. Different levels of magnetic field can be adjusted by changing the applied current to the coils.

The structure of the circuit is connected by the two steel laminates to form a flux return path. For high frequency characterization, eddy current in the structure may cause the circuit to be overheated during testing. Thus, the steel of the circuit was laminated, and insulating tape (Kapton tape) was applied between each steel layer to further reduce the effect of eddy currents. The dimensions and properties of the excitation coils are listed in Table 1.

Table 2.1: Drive coils dimensions and properties [16]

Number of Turns	Length	Resistance	Gains
1600 turns	30.48 mm (1.2 in.)	16 ohms	36.9 (kA/m)/A

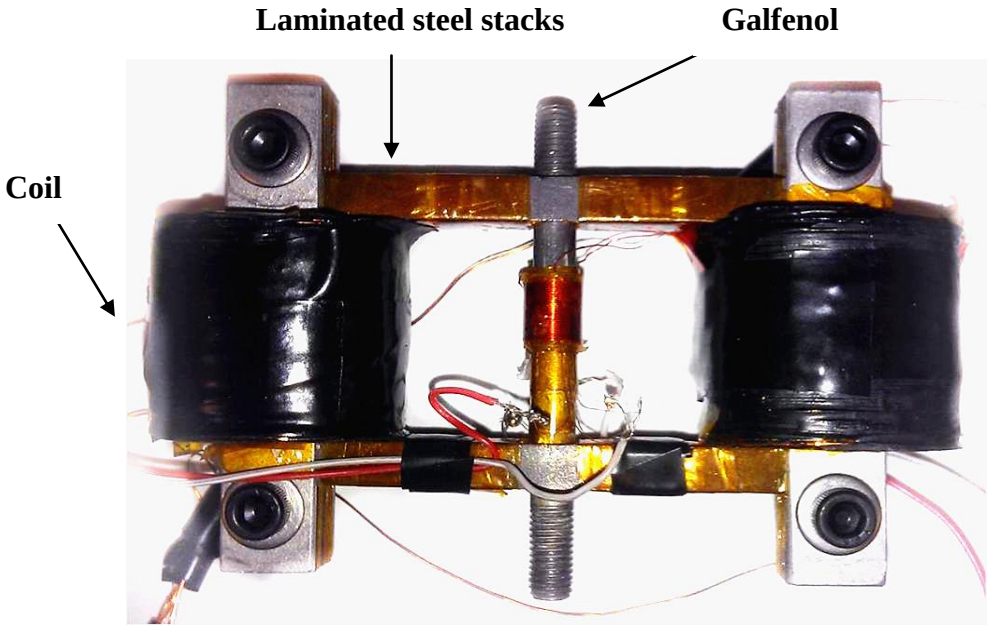

Figure 2.2: Magnetic flux circuit

2.3 Measurement System Overview

The measurement system consists of three subsystems, magnetic system, electrical system, and mechanical system. In each domain, the main parameters need to be recorded are shown in Table 2. The data acquisition device used in this measurement was LabVIEW 2012 from National Instruments Corporation. The analog input modules used are NI 9239 and NI 9237. For actuation measurements, the input sinusoidal current was generated by a NI 9263 analog output module. The overview of the measurement system is shown in Figure 2.3.

Table 2.2: Major parameters in magnetic system, electrical system, and mechanical system

Magnetic	Electrical	Mechanical
Magnetic field, H Flux Density, B	Current, I	Stress, T Strain, S

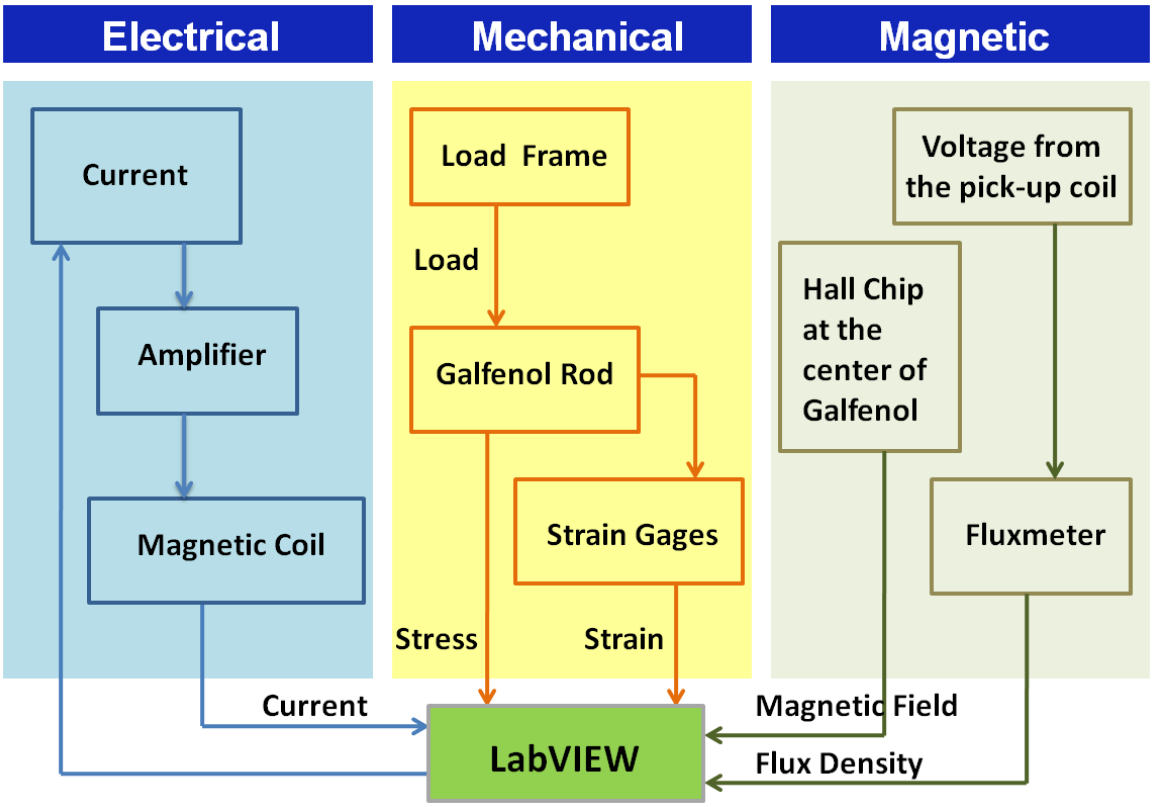

Figure 2.3: Overview of the measurement system for quasi-static characterization

2.3.1 Magnetic System

In the magnetic system, magnetic field and magnetic flux density are the two quantities of interest. The magnetic field was measured using an Allegro A1322 LUA-T Hall chip placed at the center of the Galfenol rod, perpendicular to the axial direction.

The second quantity of interest was the magnetic flux density. A pick-up coil was used to measure the flux density, which has 74 turns and an inside diameter of 6.35 mm (0.25 in.). When the magnetic flux flowed through the Galfenol sample, the pick-up coil was excited and generated a voltage. The voltage in the pick-up coil was collected and integrated by a MF-5D Fluxmeter from Walker Scientific. The flux density through the Galfenol sample then can be calculated by

$$B = -\frac{1}{NA} \int V_{pu}(t)\, dt \tag{2.1}$$

Here, B is the magnetic flux density, N represents the number of turns of the pick-up coil, A is the cross sectional area of the pick-up coil, and V_{pu} is the voltage in the pick-up coil as a function of time t. To obtain an accurate value of the term $\frac{1}{NA}$, the pick-up coil was calibrated using an annealed Nickel 200 sample with the same dimension as the Galfenol rod. The Nickel rod was placed in the magnetic circuit and the B-H curve at zero stress was measured. Finally, the value of $\frac{1}{NA}$ was calculated by that matching the experimental B-H curve with the reference B-H curve for the same Nickel sample. The calibration curve is shown in Figure 2.4. The actual NA term was calculated to be 21.296 cm^2. According to this NA value, the fluxmeter was calibrated to have a setting of 21 cm^2. A 1.4 % error of

the *NA* value still existed after the calibration. In data analysis, this error was taken into account to minimize the systematic errors.

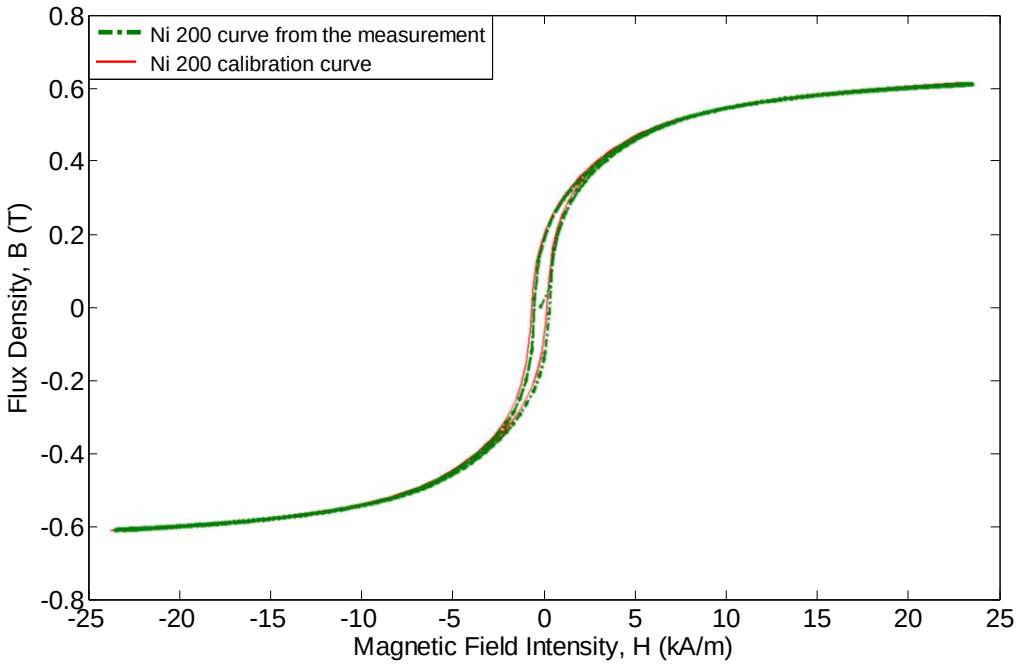

Figure 2.4: Pick-up coil calibration using annealed Ni-200 rod

2.3.2 Electrical System

The quantity of interest in the electrical system is the input current to the excitation coils. In actuation measurements, a sinusoidal current signal was generated by a NI 9263 analog output module from National Instruments, amplified by an AE Techron 5050 linear amplifier, and finally sent to the excitation coils. The current sent to the coils was monitored through LabVIEW in case the coils overheated accidentally by a high input current.

The sensing measurements were conducted with a constant excitation current applied to the drive coils. Constant current was generated by a triple-output DC power supplies from Agilent Technologies. The Hall chip used in this research was also powered by this power supplies.

2.3.3 Mechanical System

In the mechanical system, the two quantities of interest are stress and strain. A 500 lb load cell from OMEGA Engineering Inc. was used to measure the load applied on the Galfenol rod. The load was applied by a MTS axial load frame. The stress was calculated from the load through the cross sectional area of the sample. Two OMEGA (SGD-3/350-LY11) axial strain gages were bonded to the center of the Galfenol rod for strain measurements, one was installed on the front and the other one was on the opposite side. Two strain gages gave a more accurate measure of the strain in the sample. Moreover, the two strain gages can be used to check if the Galfenol rod was straight during testing. Bending of the sample could lead to problems such that the force measured from the load cell may not reflect the actual force applied on the Galfenol sample.

A schematic image of the test setup is shown in Figure 2.5, and Figure 2.6 depicts the actual test setup. On the top side, the Galfenol rod was directly affixed to the standard rod of the load frame, which formed a rigid structure and minimized the transmission loss. On the bottom side, the Galfenol rod was connected to the base of the load frame, adapted through an aluminum plate. This setup aided in aligning the sample with the axial loads and increased the accuracy of the measurements.

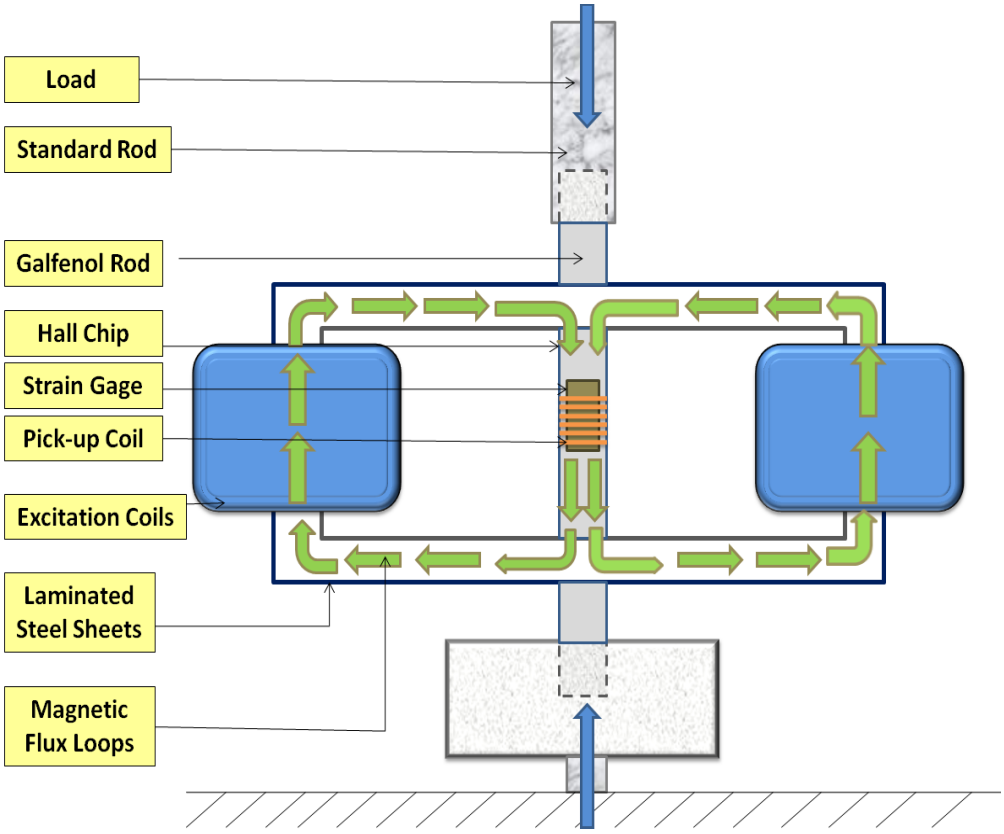

Figure 2.5: Schematic of test setup for quasi-static characterization

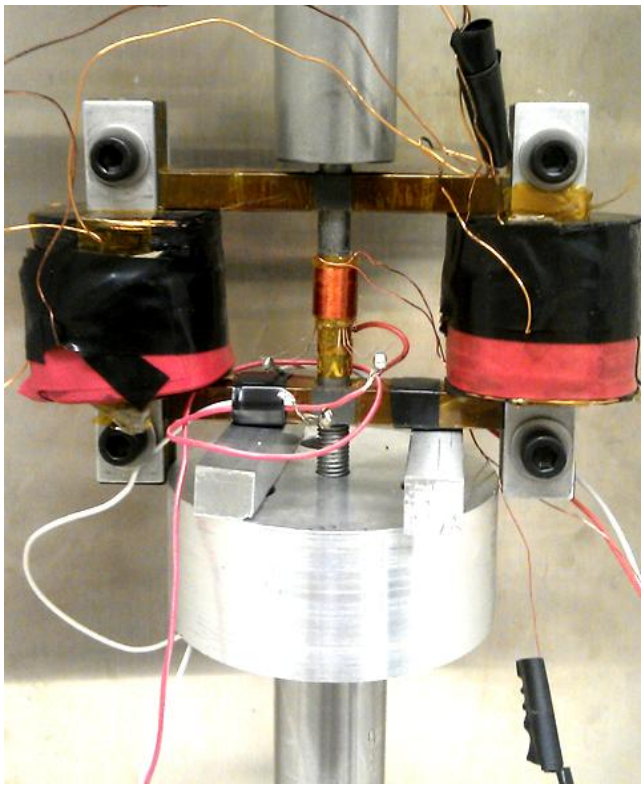

Figure 2.6: Test setup for quasi-static characterization

2.4 Inverse Effect (Actuation) Measurements

In this section, the actuation measurements are discussed along with the experimental results. The actuation behavior was analyzed based on flux density versus field (B-H) and strain versus field (S-H) curves. The tests were conducted by applying a 0.1 Hz, 22 kA/m amplitude sinusoidal magnetic field at different constant bias stress levels. The magnetic field was applied using the magnetic circuit discussed in section 2.2. The constant stress ranged from 0 MPa to – 60 MPa at 10 MPa intervals. A quick strain test was conducted before each measurement to check if the Galfenol sample was bended at the bias compressive stresses. The measurements were not run until the readings of the two strain gages were quite close, 10% error or below.

Flux density versus field curves at different stress levels are shown in Figure 2.7. The B-H curves can be divided into three main sections. The first section is characterized by the linear regions in flux density at very low magnetic fields. The second section is characterized by the burst region in flux density at a higher magnetic field, and the third region is defined by the saturation behavior at a high magnetic field. Saturation is where the curves become flat and there is no change in flux density as the field increases. It can be noticed that flux density reaches a same saturation (~ 1.48 T) at various constant stress levels. As the compressive stress increases, a higher magnetic field is needed to saturate the Galfenol sample. Another noticeable behavior is that the slope of the first section of the curve decreases with increasing stress as well as the burst region in the second section.

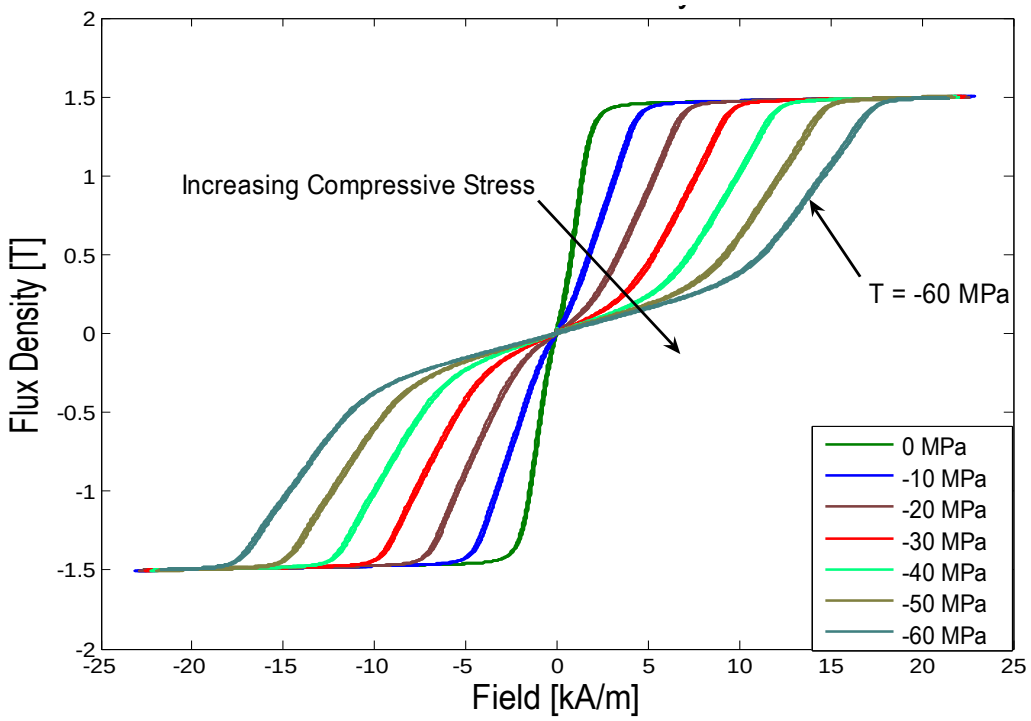

Figure 2.7: Flux density vs. field at bias stresses of 0, -10, -20, -30, -40, -50, -60 MPa

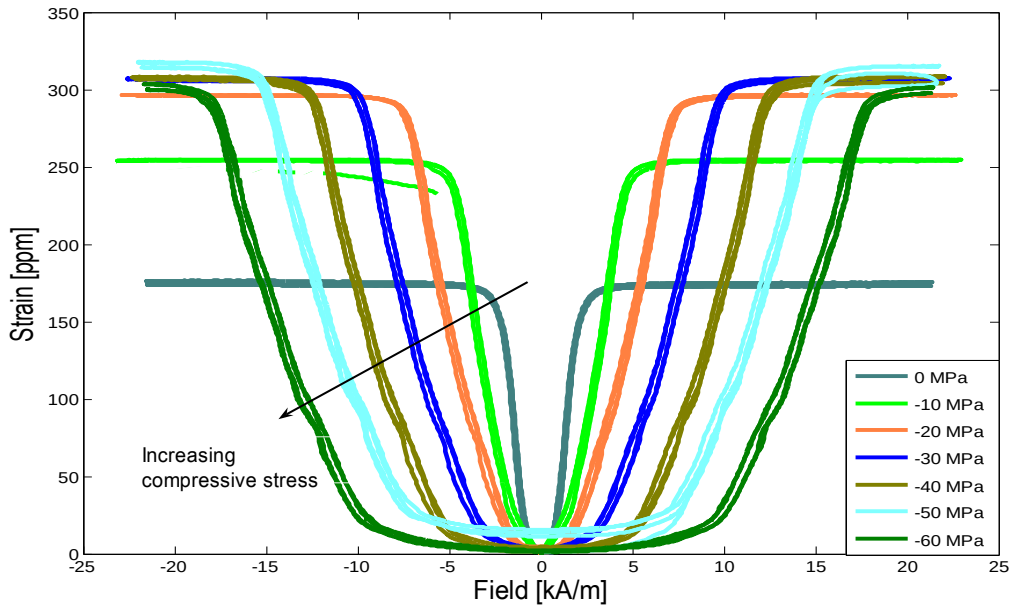

Figure 2.8: Strain vs. field at bias stresses of 0, -10, -20, -30, -40, -50, -60 MPa

The strain versus field curves at different bias stresses are shown in Figure 2.8. The S-H curves can be divided into two main sections. The first section is characterized by the burst region in strain at low magnetic fields, and the second section is characterized by the saturation behavior at a high field. As the compressive stress increases, a higher magnetic field is required to saturate the Galfenol sample. The saturation magnetostriction increases with increasing compressive stress up to ~23 MPa. The saturation magnetostriction stays the same (~300 ppm) with increasing compressive stress higher than 23 MPa. This is where all the magnetic domains are aligned with applied field.

It was noticed that the saturation magnetostriction was slightly higher as compared to the value previously measured by Walker [25], which was approximately 280 ppm. To further validate the results, a strain measurement was conducted using a laser displacement sensor. The strain measurement is discussed in section 2.4.1.

2.4.1 Strain Measurement with Laser Displacement Sensors

This section has focused on the strain measurement of the Galfenol sample using a laser displacement sensor from Keyence Corporation. The experimental setup is shown in Figure 2.9. An aluminum cylinder was machined to provide a reference surface for the reflection of the laser beam. The laser emitter was supported by a rigid structure with 25.4 mm (1 in.) higher from the reference surface, and the strain was measured as the aluminum cylinder moved up and down. Actuation measurements at a compressive stress of 40 MPa were conducted at four different positions, which reduced the systematic error and increased the experimental accuracy.

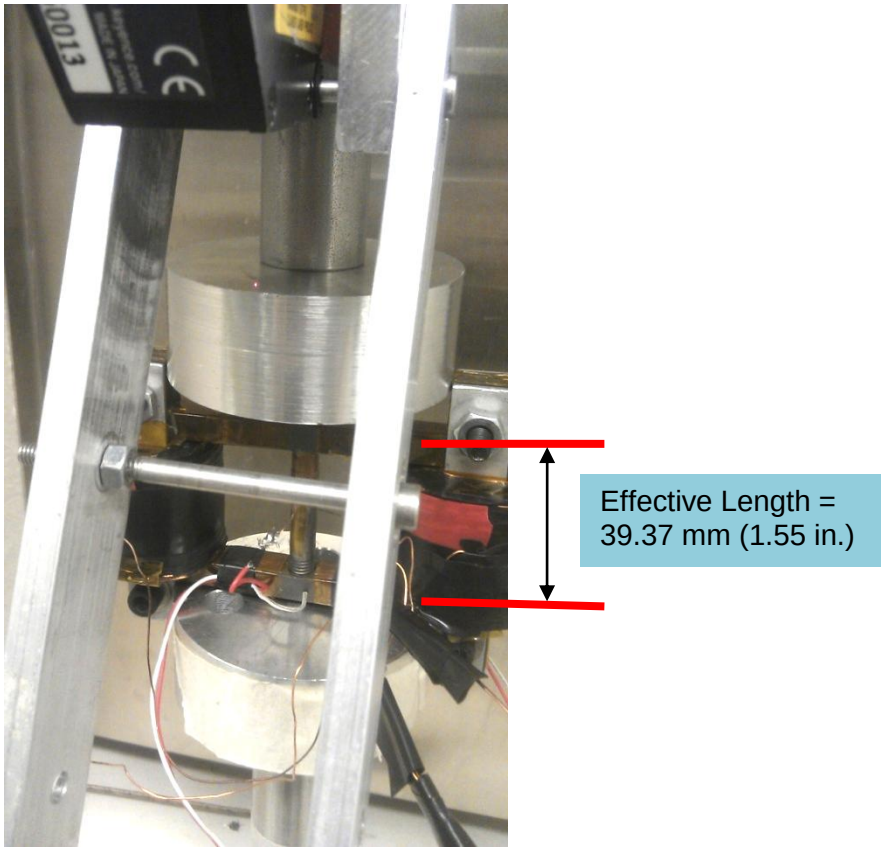

Figure 2.9: Test setup for the strain measurement using a laser displacement sensor

The results of the strain measurement are shown in Figure 2.10 and Figure 2.11. The saturation magnetostriction at four different positions was 299.7 ppm, 295.1 ppm, 301.1 ppm, 299.4 ppm, respectively. The mean value was 299.0 ppm. The mean saturation was very close to the saturation magnetostriction, which was 303.5 ppm. The difference was 4.5 ppm and approximately 1.5 % error. Therefore, the saturation magnetostriction measured in section 2.4 can be validated.

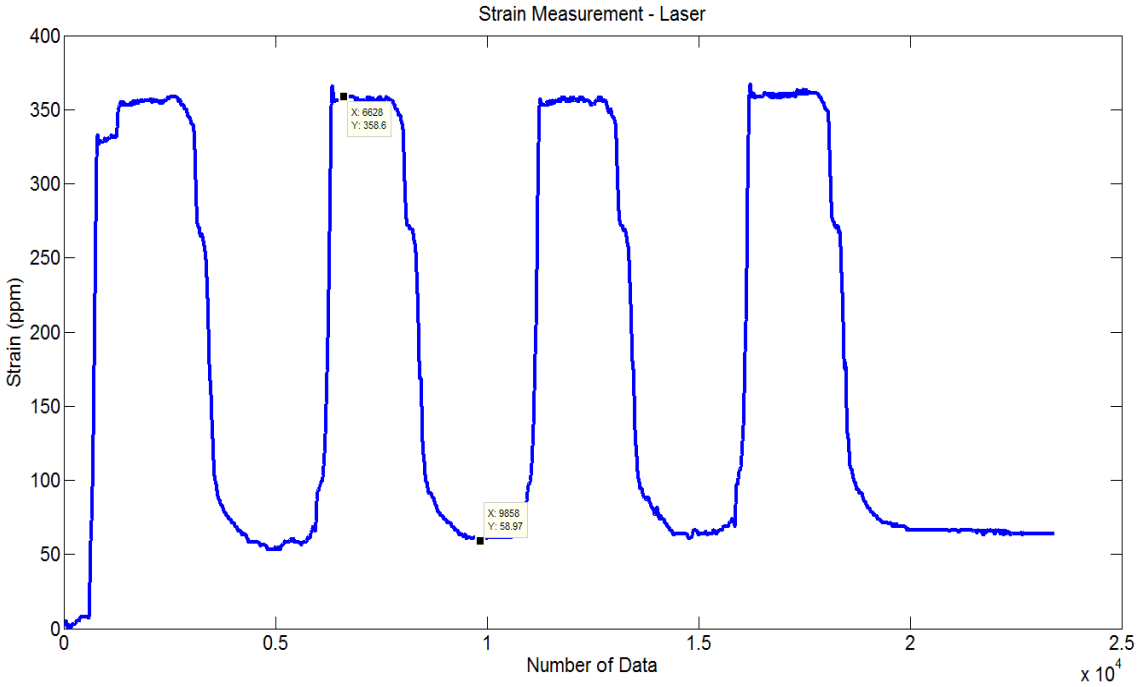

Figure 2.10: Strain vs. time at a bias stress of -40 MPa using a laser displacement sensor

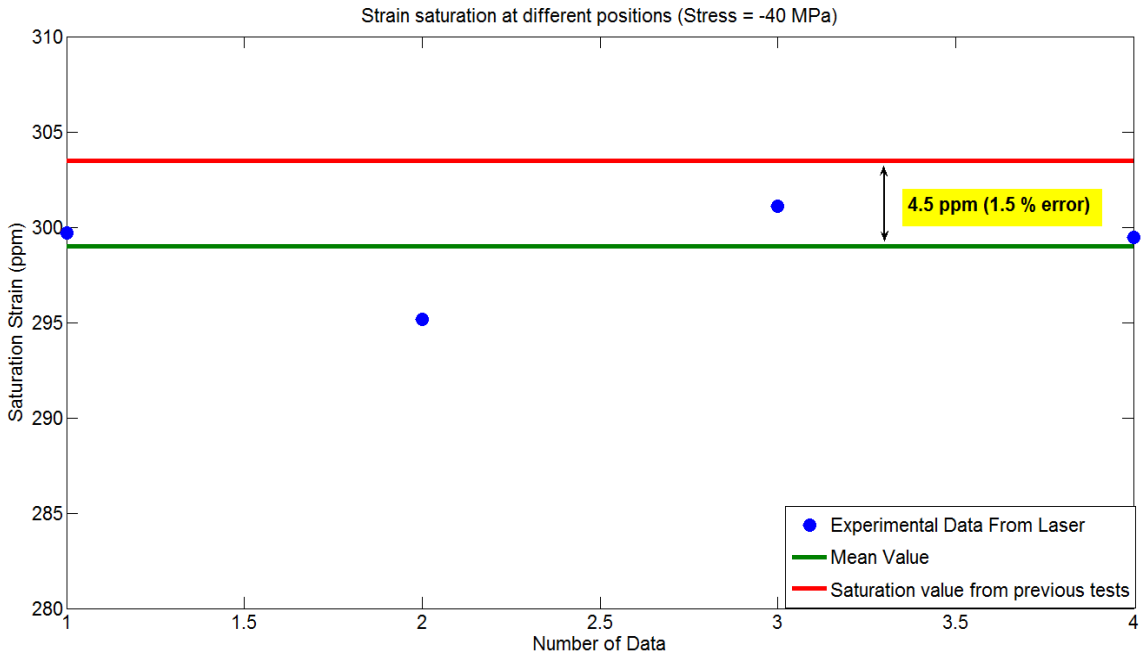

Figure 2.11: Comparison of saturation magnetostriction between measurements using strain gages and using laser displacement sensors

2.5 Direct Effect (Sensing) Measurements

The sensing behavior was characterized based on the direct effect of magnetostrictive materials. The sensing measurements were conducted by applying a sinusoidal stress signal at different bias fields. A bias field was set by applying a constant current to the excitation coils. The constant current ranged from 100 mA to 850 mA at 50 mA intervals. In sensing measurements, flux density versus stress (B-T) and strain versus stress (S-T) measurements were conducted and discussed. In constant current mode, the field did not exactly track the current due to the change in the permeability of the Galfenol sample. Thus, field versus stress curves were also monitored and analyzed.

2.5.1 Major Loop Tests

Major loop tests were conducted with a wide range of input stresses. The major loops can be used in the modeling of Galfenol-based transducers. In major loop tests, the first step was to bring the Galfenol sample to a desired bias field by adjusting the current to the excitation coils. The biasing procedure consisted of applying a 1 A current to the coils and then decreasing to the desired excitation current. The Galfenol sample was pre-stressed to a bias stress of -31 MPa, and then a 0.05 Hz, 31 MPa amplitude sinusoidal stress input was applied to the material.

Figure 2.12 shows the major flux density versus stress loops with different constant currents to the excitation coils. There are two noticeable characteristics of the major flux density versus field loops. First, the burst region shifts to the left at a higher excitation current. At this location, domains aligned along the field are forced to rotate perpendicular to the direction of the compressive stress. In other words, the domains start rotating and flipping as the stress is large enough to overcome magnetic field and anisotropy energy. The second notable characteristic is that the saturation of flux density increases as the constant current increases. The saturation indicates that all of the magnetic domains are aligned perpendicular to the direction of the stress. The difference in saturations is due to the fact that the strength of the magnetic energy works against the stress. Besides, a small magnetization is produced by the bias field at a high stress.

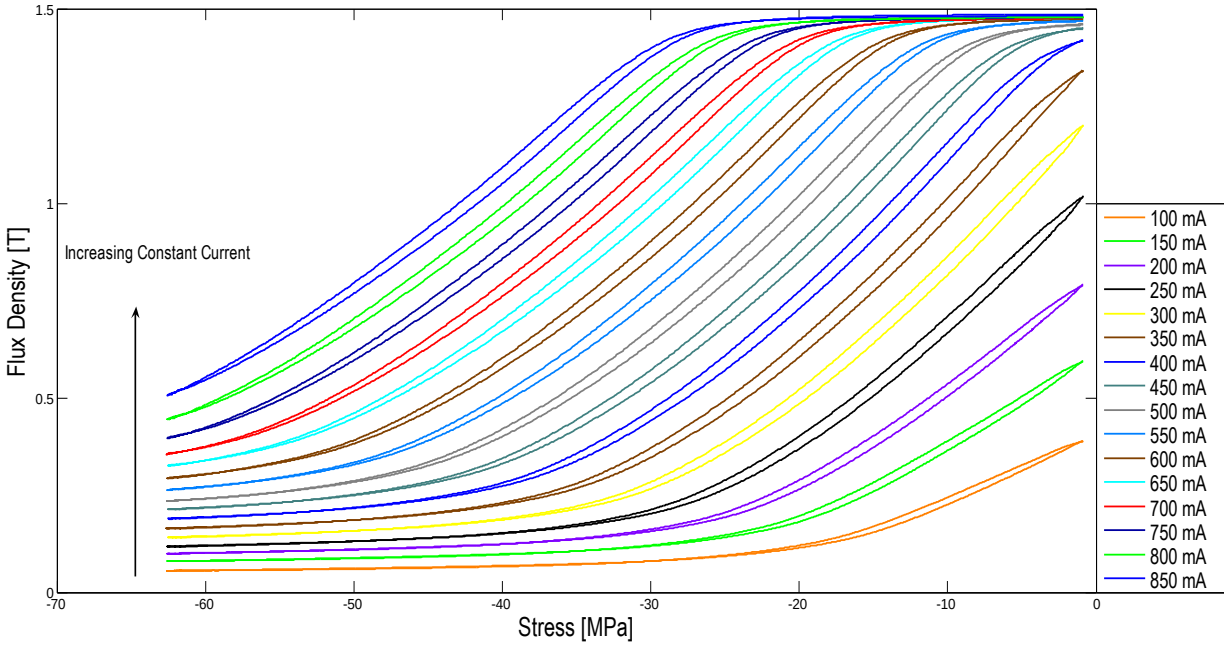

Figure 2.12: Flux density vs. stress for major loops with constant current excitation

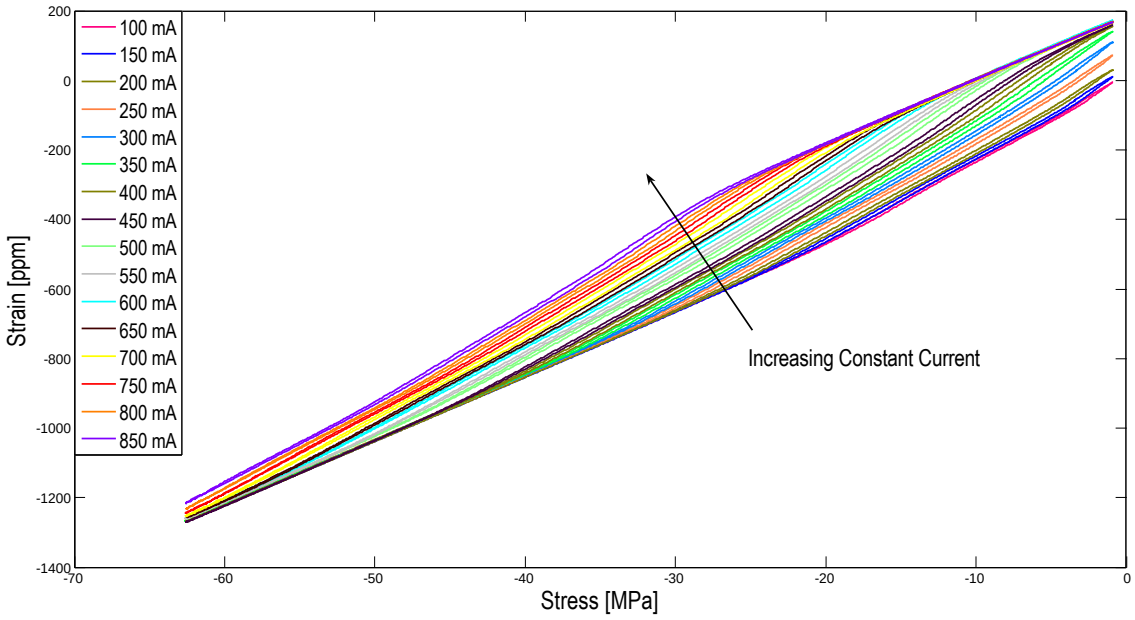

Figure 2.13: Strain vs. stress for major loops with constant current excitation

Figure 2.13 shows major strain versus stress loops with different constant currents to the excitation coils. Similarly, the nonlinearity of the magnetostriction curves is caused by the interplay between the mechanical and magnetic energy regimes. The strain response is dominated by magnetic effects at low stresses, and by mechanical effects at high stresses.

Figure 2.14 shows magnetic field as a function of stress with different constant currents applied to the drive coils. It can be noticed that the magnetic field is not constant as stresses are applied. This behavior is caused by the nonlinearity between the applied current and the magnetic field, and between the reluctance of the circuit and the magnetic field. In the Evans and Dapino model [15], input-output relations are quantified so current can be taken as an input so constant magnetic field is not necessary.

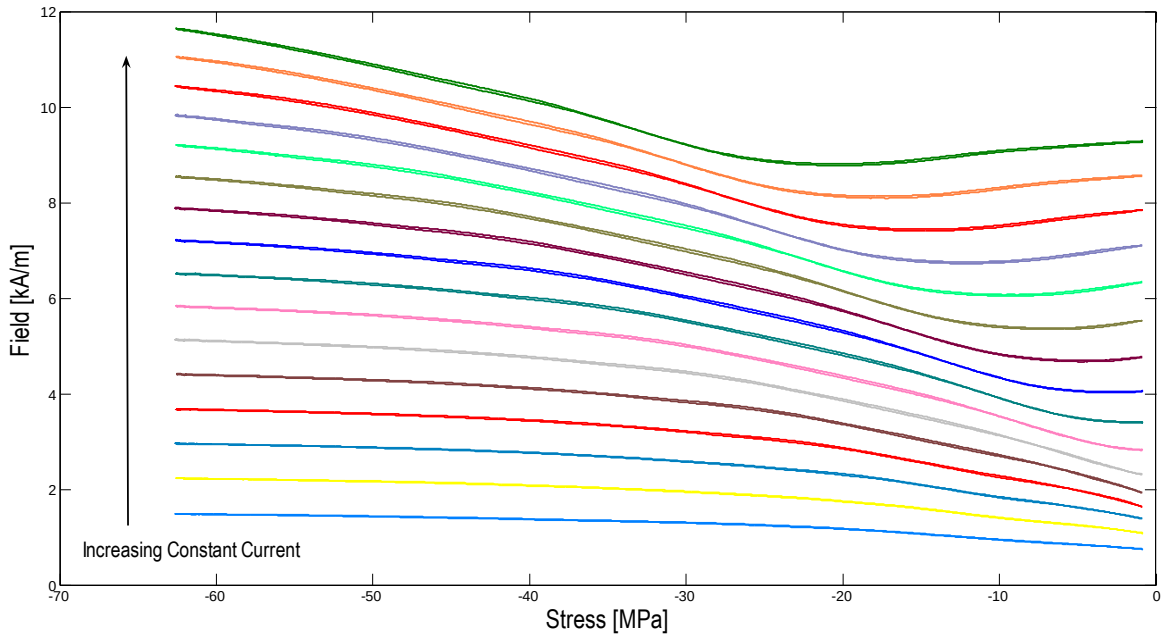

Figure 2.14: Field vs. Stress for major loops with constant current excitation (same current values as Figure 2.12 and 2.13)

2.5.2 Minor Loop Tests

Minor loops aid in implements of Galfenol in practical applications. In real world environment, Galfenol often operates within a small range of stress due to its nonlinear behavior. Responses in the linear region enable Galfenol to be used for an accurate and quick implementation. Also, minor loop measurements allow for a comparison between major loops and minors loops, which will further validate the accuracy of the results.

Similar to the major loop measurements, a constant current was applied to the drive coils. The constant currents were applied ranging from 100 mA to 650 mA in 50 mA steps. The Galfenol sample was first subjected to a 2224 N/min ramp loading to a desired stress level. Minor loops were then obtained by applying a 0.25 Hz, 4 MPa amplitude sinusoidal stress signal for three cycles. Five different bias stresses were chosen to be from -50 MPa to -10 MPa in 10 MPa increments. Figure 2.15 shows flux density versus stress for minor loops with constant current excitations. Figure 2.16 indicates strain versus stress for minor loops with constant current excitations.

The minor loops were also plotted on the top of the major loops to check if the minor loops were located inside the major loops. Through the comparison of the curves, it can be seen that the minor loops follow the major loops in trajectory so operating about a bias stress level does not change the behavior of Galfenol as well as the response of the system. Another observation is that the minor loop has a slightly lower sensitivity than that of the major loop. The variation in sensitivity is due to the small range of the applied stress. The minor loops do not have a sufficient stress range to close themselves.

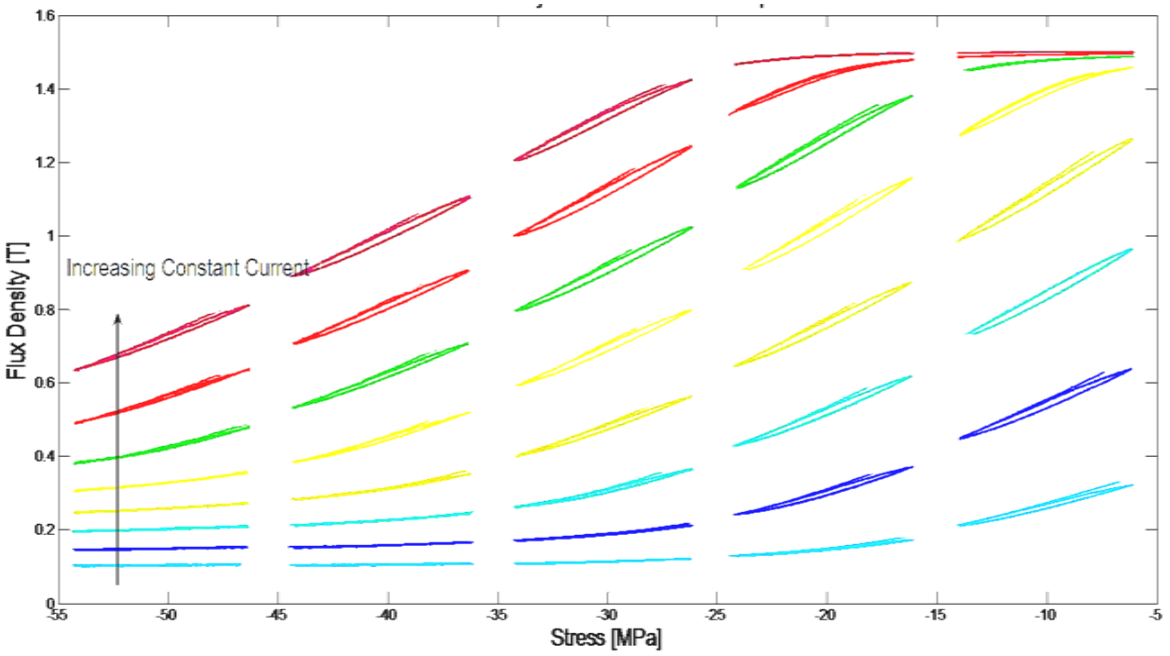

Figure 2.15: Flux density vs. stress for minor loops with constant current excitation – Bias stress (-10, -20, -30, -40, -50 MPa) with 4 MPa amplitude

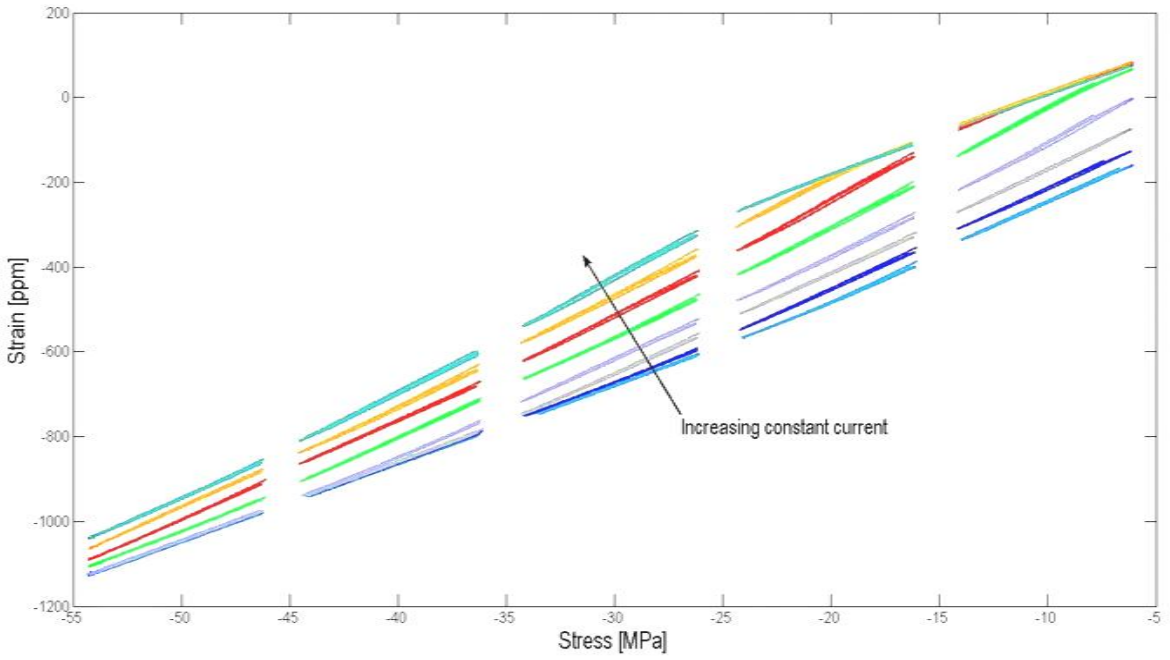

Figure 2.16: Strain vs. stress for minor loops with constant current excitation – Bias stress (-10, -20, -30, -40, -50 MPa) with 4 MPa amplitude

2.6 Analysis and Discussion

To further validate the accuracy of the results, the actuation and sensing measurements were cross-checked by plotting stress-flux density data points on top of field-flux density curves. The result is shown in Figure 2.17.

Sensitivity determines how much change in output corresponds to unit input, which is the basis in designs of sensors. Sensitivity versus stress curves for major loops can be seen in Figure 2.18. Figure 2.19 indicates the comparison of sensitivity between the major loops and minor loops. The sensitivity of major loops was calculated by dividing the curve into sixteen equal intervals and taking the average of the sensitivity of the upper and lower portion of the loop in each interval. The sensitivity of minor loops was approximated using first order polynomial method. The sensitivity of minor loops is lower than from major loops because of the variation in the slope of minor loops.

Elastic modulus is defined as the ratio of stress to strain, and it can be used to calculate the elastic deformation as a force is applied to the material. The variability of elastic modulus in Galfenol is important in the performance and modeling of Galfenol transducers. Elastic modulus as a function of stress for major loops is shown in Figure 2.20. Figure 2.21 shows the comparison of modulus of elasticity between major loops and minor loops. Calculations for elastic modulus were similar to calculations for sensitivity. The elastic modulus from minor loops is consistently higher than from major loops due to the change in the slope of minor loops.

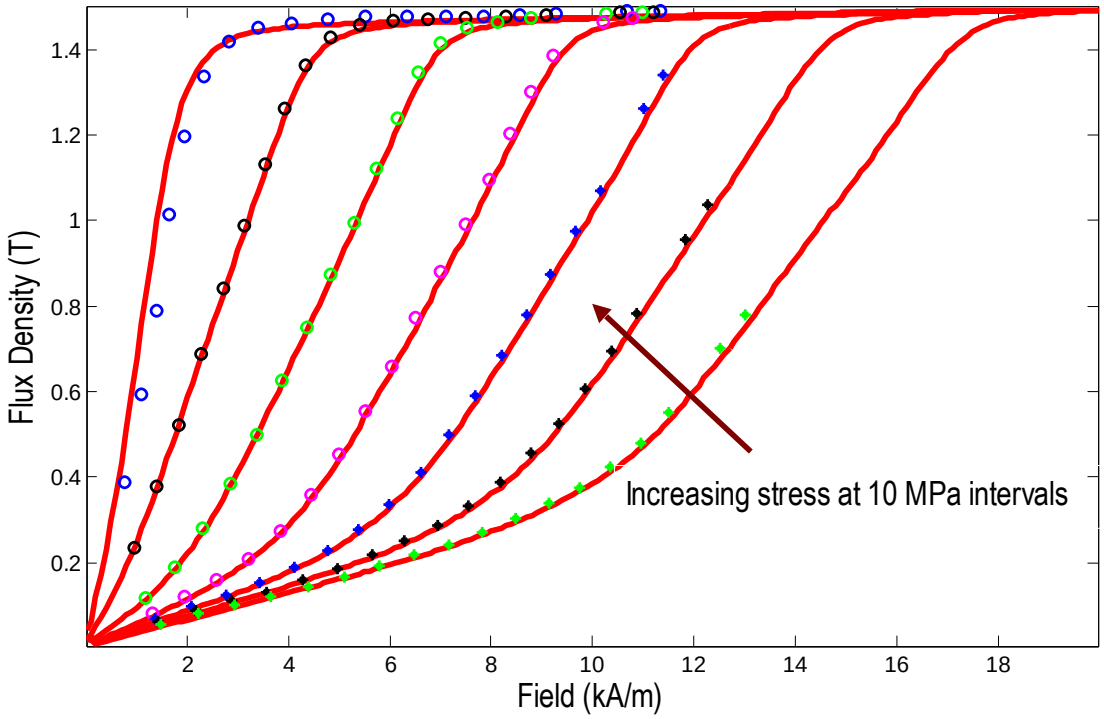

Figure 2.17: Anhysteretic averages for flux density versus field curves (red lines) and flux density versus stress data points (dots)

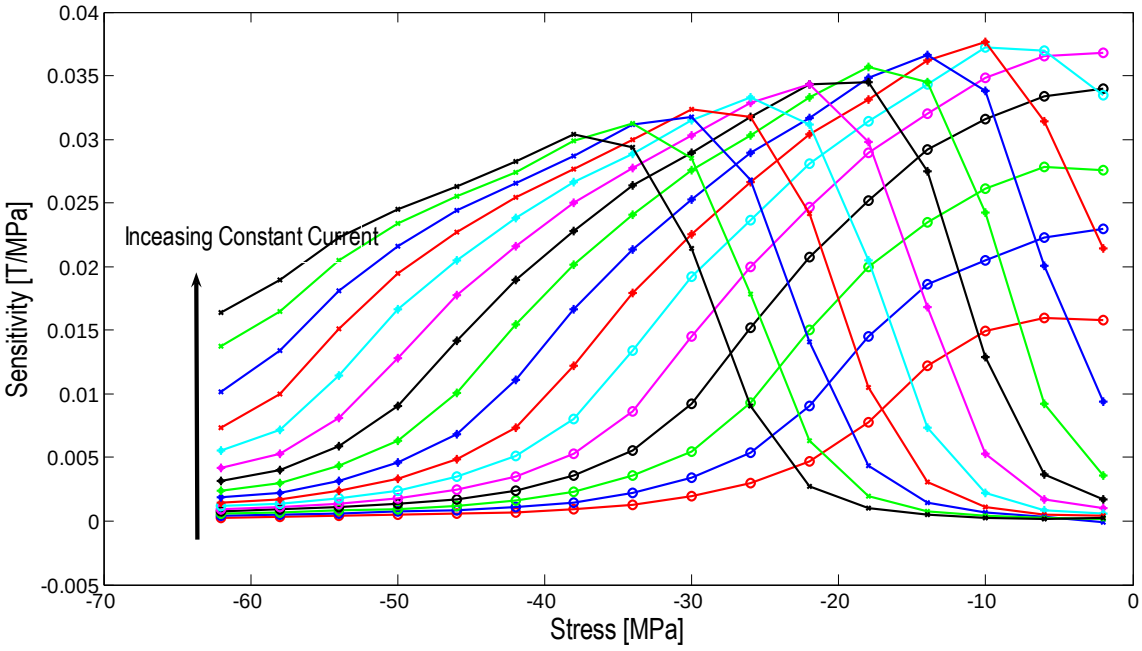

Figure 2.18: Sensitivity versus stress for major loops with constant current excitation

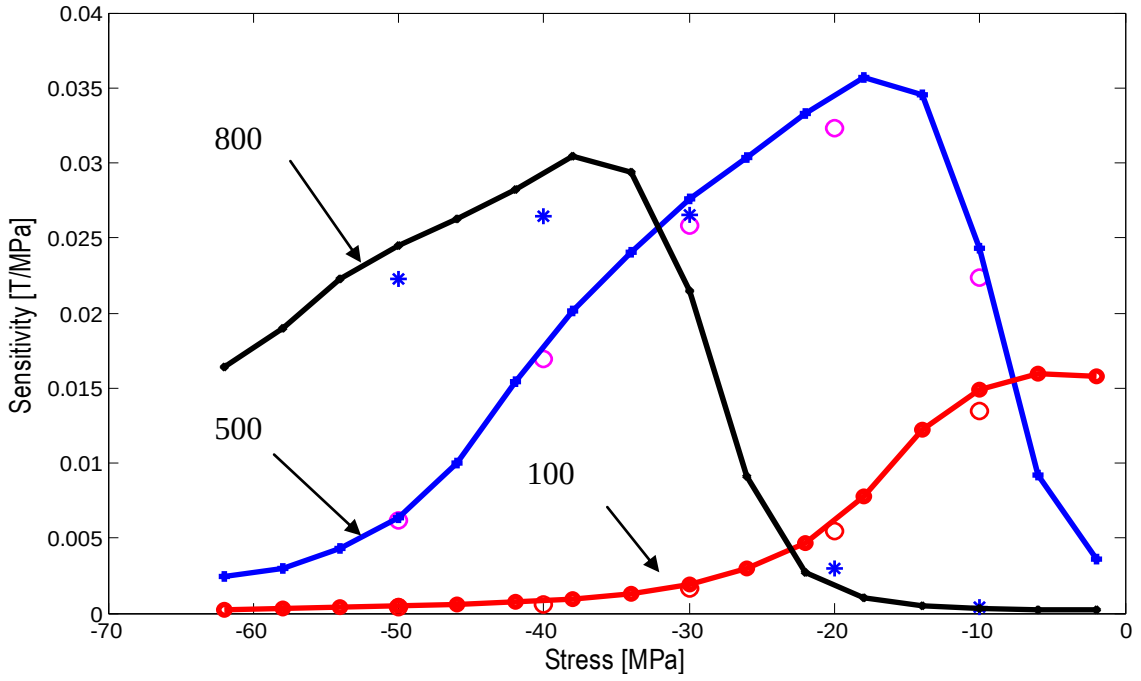

Figure 2.19: Sensitivity vs. stress for minor and major loops with constant current excitation - lines: major loops; dots: minor loops

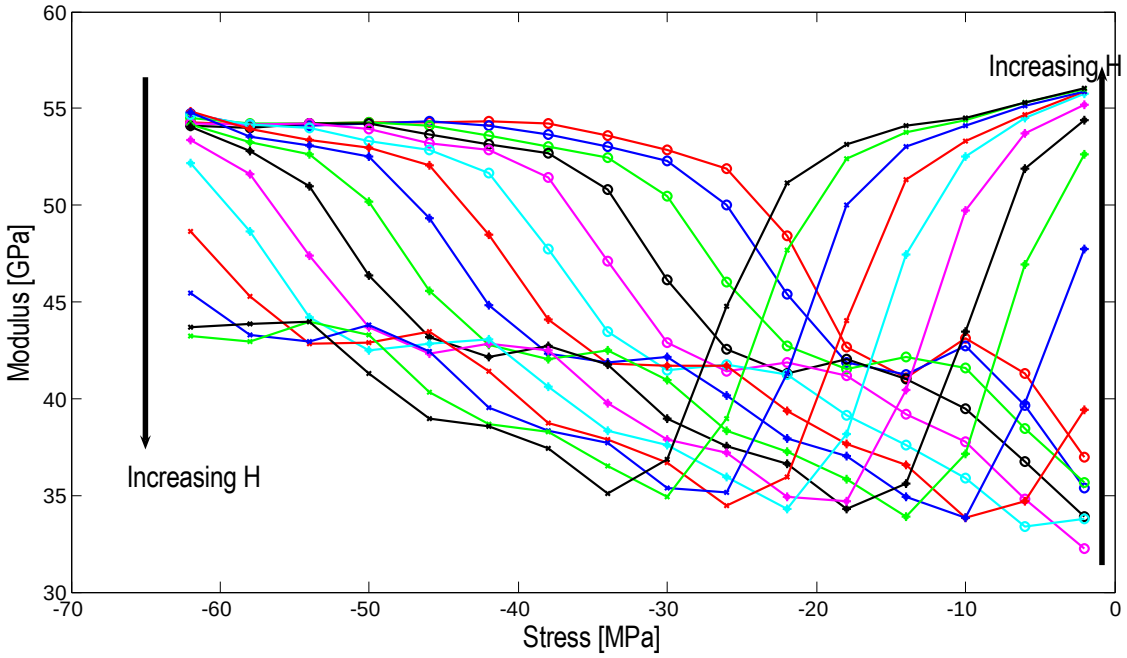

Figure 2.20: Elastic modulus versus stress for major loops with constant current excitation

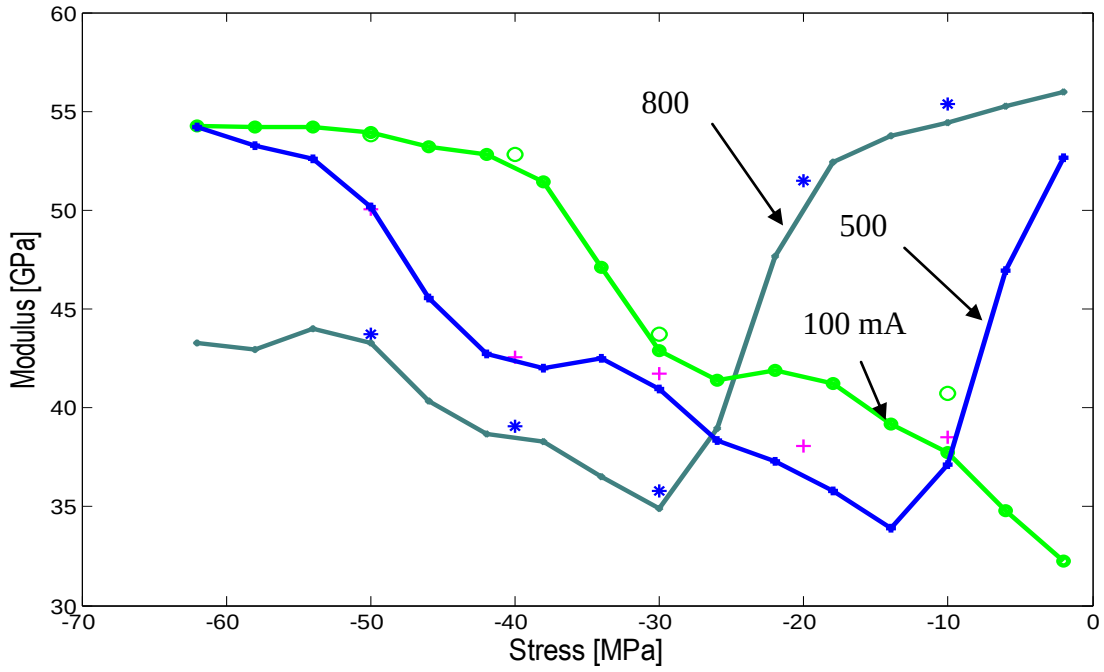

Figure 2.21: Elastic modulus vs. stress for minor and major loops with constant current excitation - lines: major loops; dots: minor loops

CHAPTER 3

DYNAMIC CHARACTERIZATION FOR SENSING

3.1 Overview

Sensors are typically used over a range of frequencies. This high-frequency characterization gives a better understanding of Galfenol's behavior under dynamic conditions. The objective of this measurement is to characterize the sensing behavior of Galfenol with different excitation frequencies, and to investigate how frequency of the input stress signal affects the output, flux density, strain, and magnetic field. These rate-dependent responses would optimize a constitutive Galfenol model and create a guideline for implementing Galfenol in force sensing applications.

There has been nearly much research in dynamic characterization of Galfenol alloys. Previous work has completed by Poeppelman [16] on characterization of Galfenol under dynamic conditions for actuation. Walker [25] has expanded the knowledge for the sensing characteristics. The dynamic characterization in this research has focused on the sensing behavior in both flux density versus stress and strain versus stress curves. Moreover, measurements with a wide range of input frequency were conducted to give a better understanding of the material's characteristics in the dynamic regime.

3.2 Test Setup

The overall measurement system can be divided into three sub-systems, which are an electrical system, a mechanical system, and a magnetic system. A schematic image of the measurement system is shown in Figure 3.1.

In the electrical system, a piezoelectric actuator was used to produce a high-frequency force input because of its linear relationship between the input voltage and output displacement. The input force to the Galfenol sample was achieved by preventing the displacement of the push rod of the actuator. The actuator is a PSt 1000/16/80 VS25 from AmericanPiezo, Inc, which has an operating range of 0-1000 V. To excite and control the actuator, the current applied to the actuator must be large. Thus, a RCV1000/7 switching amplifier from AmericanPiezo was used to amplify a small voltage signal produced from LabVIEW. The sensing measurements were conducted with constant currents applied to the drive coils using a power supplies from Aglient Technologies. The constant excitation current was chosen to be 500 mA. In the mechanical system, a SN 22276 – 208C02 load cell from PCB Piezotronics, Inc. was used to capture the high-frequency forcing signal applied on the Galfenol sample. The magnetic system was the same as in the quasi-static characterization. Details have been discussed in section 2.3.1.

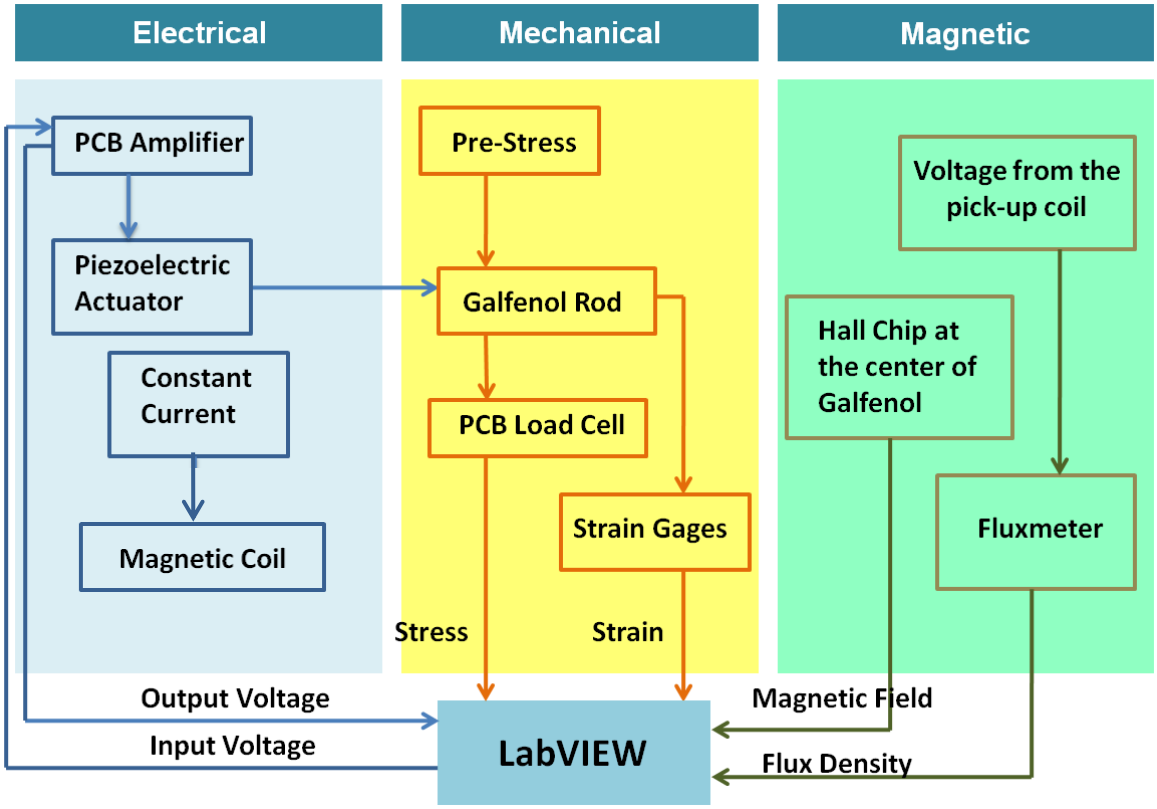

Figure 3.1: Overview of measurement system for dynamic characterization

The test setup is shown in Figure 3.2. For clarity, a schematic of the setup can be seen in Figure 3.3. The entire setup was built on an isolation table to avoid vibration effects during testing. Two steel adapters were machined, one for adapting the actuator to the Galfenol sample, and one for creating a large surface area for the actuator to push on. The setup made use of two stiff steel supports, one on each side to create a rigid structure. The supports were secured when the supports, the actuator, and the Galfenol rod were aligned. This rigid structure allowed the force generated in the actuator to be applied to the Galfenol sample, and to minimize the transmission loss.

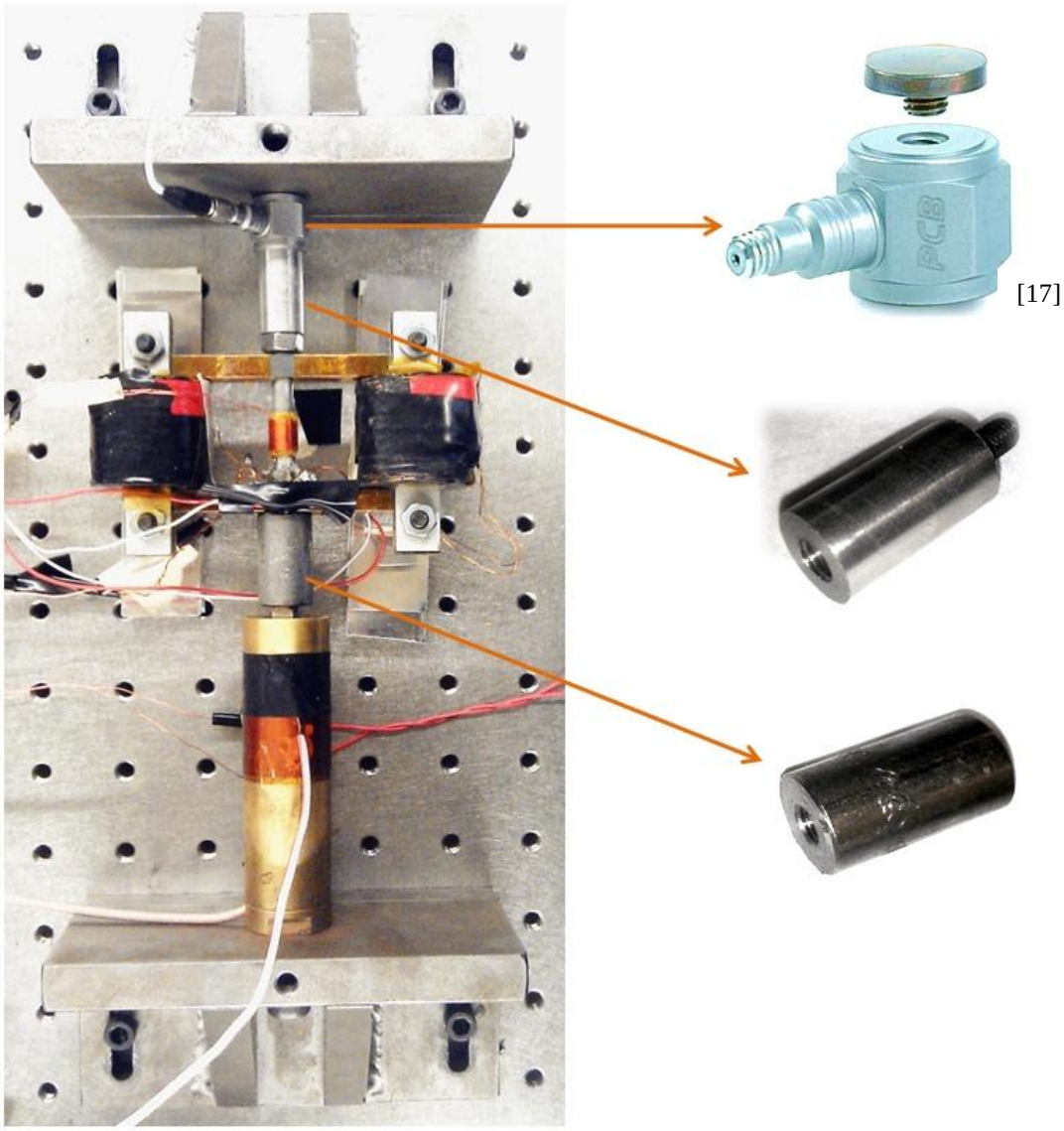

[17]

Figure 3.2: Test setup for dynamic characterization

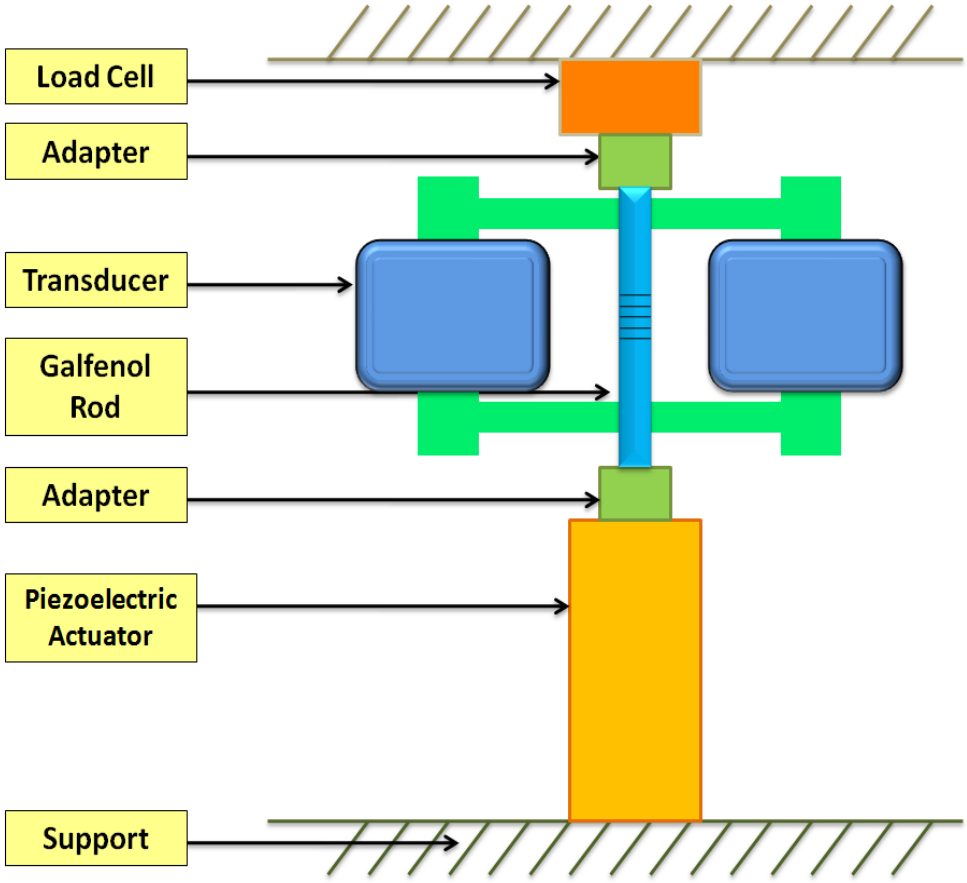

Figure 3.3: Schematic of test setup for dynamic characterization

3.2.1 Compliance Analysis

The stiffness of each component in the system has an impact on the force transmitted to the Galfenol sample. The compliance of the components would reduce the force transmission because of the energy loss in deforming these components. The force applied on the Galfenol is caused by the displacement of the piezoelectric actuator, which has a maximum of 80 μm. In order to maximum the force transmission, each component in the path of the applied force needs to be stiffer than the Galfenol rod. In other words, the two supports, the load cell, and the two adapters must have a minimum displacement, and thus a high force can be achieved through the Galfenol rod. Therefore, the stiffness of the frame structure was analyzed and compared to the stiffness of the Galfenol rod.

Table 3.1 lists the dimensions and stiffness of each component in the dynamic characterization setup. The stiffness was calculated using Equation 3.1.

$$k = \frac{AE}{L} \tag{3.1}$$

The ratio of the stiffness of each component to that of the Galfenol was also analyzed. It can be seen from the table that the components are stiffer than the Galfenol sample, so Galfenol would exhibit a much larger displacement when a force is applied. A schematic of the simplified model is shown in Figure 3.4. In the path of the applied force, the components were connected in series so the stiffness on each side can be calculated, as shown below.

Table 3.1: Stiffness of the components in the dynamic characterization setup

Element	Cross Sectional Area(m^2)	Length(m)	Elastic Modulus (GPa)	Stiffness ki (N/m)	$\frac{ki}{k\_Galfenol}$
Galfenol Rod	3.167×10^{-5}	0.047	55	3.7×10^{7}	1.00
Actuator	X	X	X	9.00×10^{7} (Data sheet)	2.43
Adapter 1	9.5×10^{-5}(1/4-28) 1.09×10^{-4}(10-32)	0.011938 (1/4-28) 0.01143 (10-32)	193	8.37×10^{8}	22.62
Adapter 2	9.5×10^{-5}(1/4-28)	0.011938 (1/4-28)	193	9.65×10^{8}	26.08
Load Cell	1.9165×10^{-4}	0.01588	X	1.05×10^{9} (Data sheet)	28.38
Supports	X	X	X	1.07×10^{9}	28.92

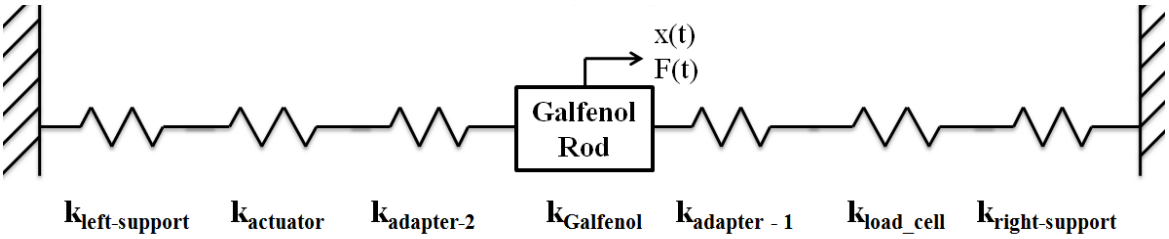

Figure 3.4: Schematic of the simplified model for dynamic characterization

- Stiffness on the left:

$$k_{left} = \frac{1}{(\frac{1}{k_{left-\text{support}}}) + (\frac{1}{k_{actuator}}) + (\frac{1}{k_{adapter-2}})}$$

$$= \frac{1}{(\frac{1}{1.07*10^{9}}) + (\frac{1}{9*10^{7}}) + (\frac{1}{9.65*10^{8}})}$$

$$= 7.64*10^{7}\ \text{N/m}$$

- Stiffness on the right:

$$k_{right} = \frac{1}{(\frac{1}{k_{\text{adapter-1}}}) + (\frac{1}{k_{load\_cell}}) + (\frac{1}{k_{right-support}})}$$

$$= \frac{1}{(\frac{1}{8.37*10^{8}}) + (\frac{1}{1.05*10^{9}}) + (\frac{1}{1.07*10^{9}})}$$

$$= 3.2*10^{8}\ \text{N/m}$$

- Stiffness of the frame structure:

$$k_{total} = k_{left} + k_{right} = 7.64*10^{7} + 3.2*10^{8} = 3.96*10^{8}\ \text{N/m}$$

$$\frac{k_{total}}{k_{Galfenol}} = \frac{3.96*10^{8}}{3.7*10^{7}} = 10.7$$

Through the calculations above, the Galfenol sample has the lowest stiffness compared to other components in the system. In addition, the stiffness of the frame structure is 10.7 times higher than that of the Galfenol sample. Therefore, the force transmission loss would be small, and a high force can be achieved on the Galfenol rod.

In high frequency tests, the frequency of the input stress ranged from 1 Hz to 800 Hz. The frequency response of the system was analyzed in order to ensure that the entire structure would not be excited during testing. Finite element analysis was conducted using the software package COMSOL. The simulation was used to analyze the natural frequency of the test setup. The simulation showed that the natural frequency of the setup was 1043 Hz. Therefore, the test setup would not be excited even at an 800 Hz input frequency.

3.3 Direct Effect (Sensing) Measurements

In Galfenol-based sensors, Galfenol must be pre-stressed to a stress level and operate within a desired region. This is due to the fact that the sensing response of Galfenol alloys is apparent at the burst region of the major loop where the mechanical effects dominate the overall response. Thus, the Galfenol sample must be pre-stressed to a critical stress level before testing.

Since PCB (208C02) load cell can only measure dynamic forces, adjusting the pre-stress on the Galfenol sample then became a critical issue. The method adapted was making use of the major flux density vs. stress loop from the quasi-static test. Once the pre-stress was adjusted, a reading was then taken from the fluxmeter. The corresponding stress

level from the major flux density vs. stress loop was found to check if the desired stress level was reached. The initial displacement of the actuator is determined by the offset of the input voltage, and the pre-stress applied on the Galfenol rod depends on the displacement of the actuator. Thus, the pre-stress can be adjusted by changing the offset of the input voltage. Figure 3.6 shows the procedures of the pre-stress adjustment.

The location of the burst region varies under different constant current excitations. A 500 mA constant current was applied to the excitation coils in this measurement. By using the major flux density vs. stress loop, the bias stress was then adjusted to -19.85 MPa, and the corresponding flux density was 1 T.

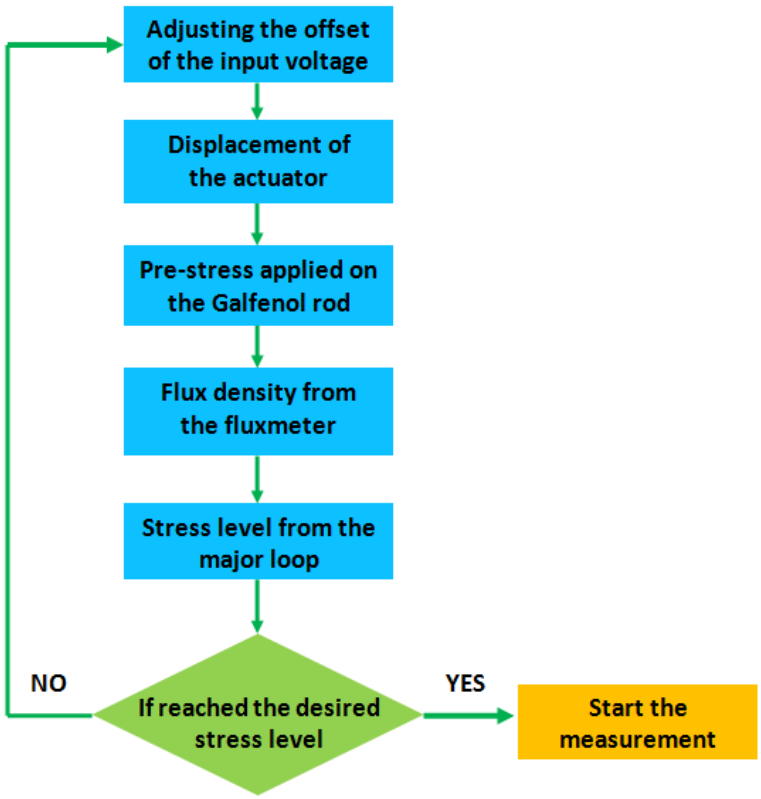

Figure 3.5: Procedure for pre-stress adjustment

In this measurement, minor loops of flux density vs. stress, strain vs. stress, and field vs. stress were tested and analyzed. Major loops under quasi-static conditions were utilized to validate the testing apparatus for dynamic characterization. This step was performed by plotting minor loops on top of major loops to check if the minor loops were located within the major loops. The validation results are shown in Figure 3.6. A 200 V sinusoidal voltage signal was applied to the actuator, which was superimposed on top of the voltage offset. This voltage signal caused a stress signal with an amplitude of approximately 3 MPa. The measurements were conducted with a focus on the stress input frequency of 5Hz, 10 Hz, and 50 Hz to 800 Hz at 50 Hz intervals. Minor loops for seven different stress excitation frequencies are shown in Figure 3.7, Figure 3.8, and Figure 3.9. A comprehensive set of results can be found in the appendix. During testing, a noticeable observation was that stress amplitude decreases with increasing frequency of the stress signal. This behavior was caused by the interaction of the components in the path of the applied force. Thus, the voltage to the amplifier was adjusted to have the minor loops with a consistent amplitude.

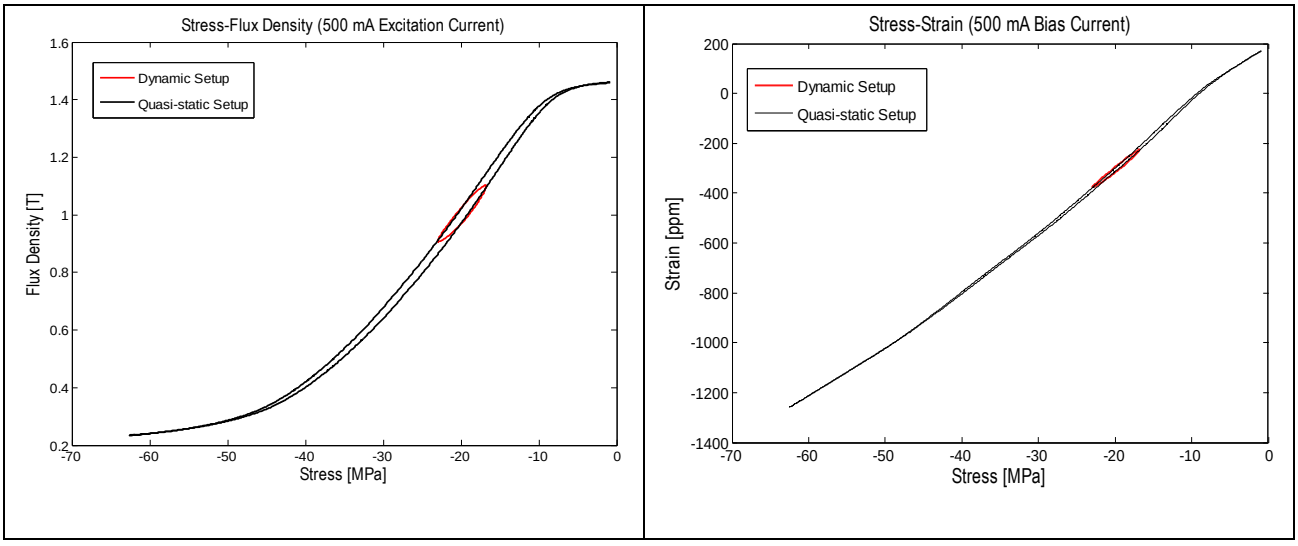

Figure 3.6: Testing apparatus validation with quasi-static results (major loop: 0.05 Hz; minor loop: 5 Hz)

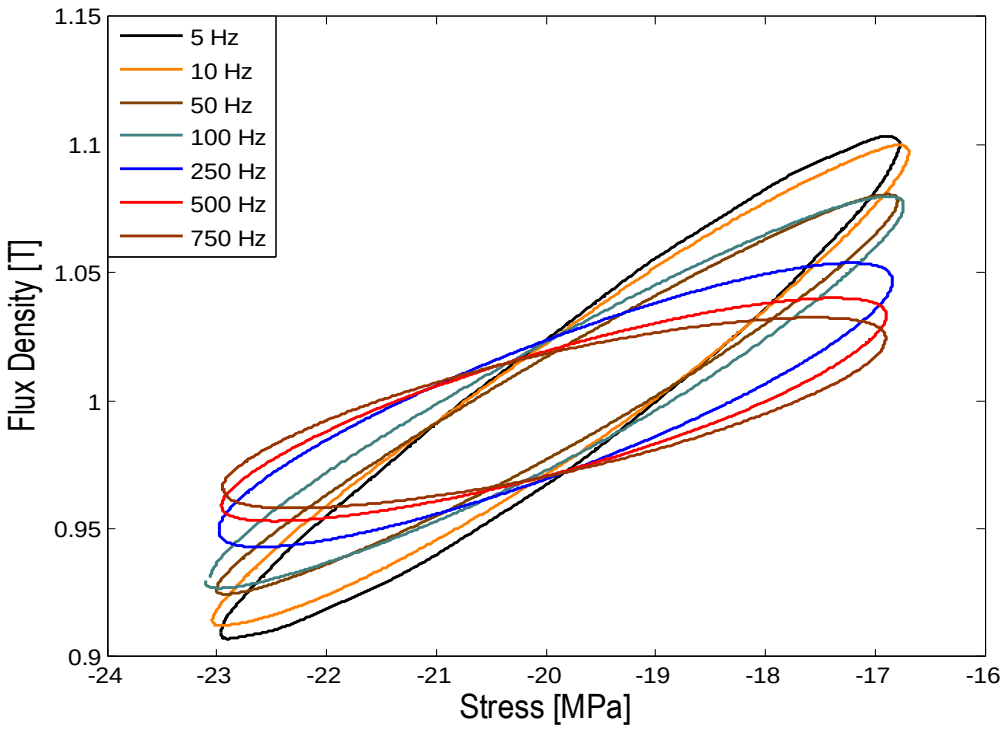

Figure 3.7: Flux density versus stress for seven frequencies (5, 10, 50, 100, 250, 500, 750 Hz) with 500 mA constant current excitation

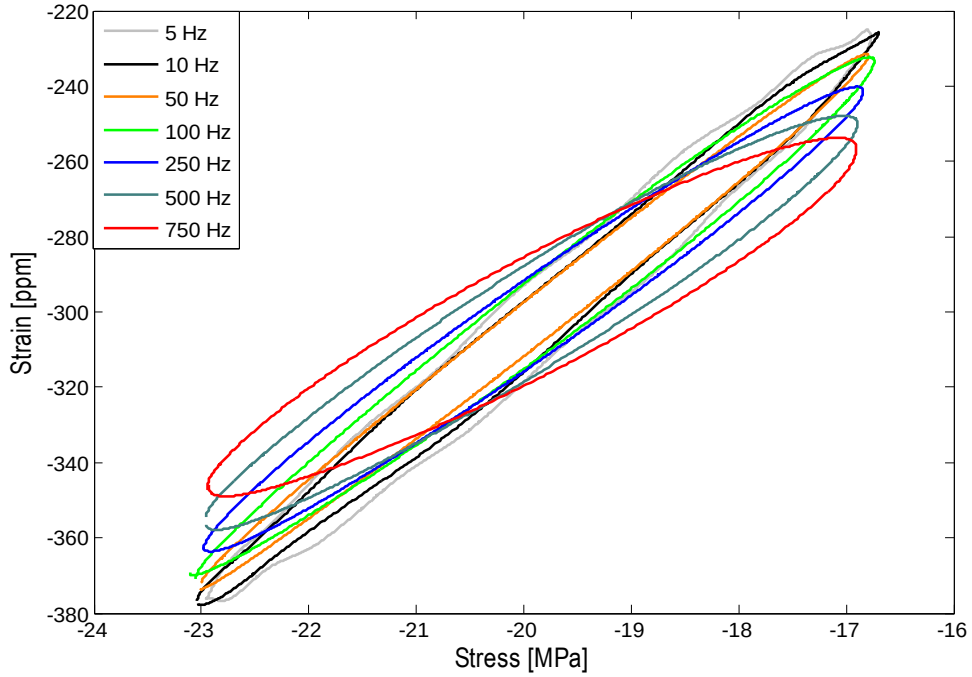

Figure 3.8: Strain versus stress for seven frequencies (5, 10, 50, 100, 250, 500, 750 Hz) with 500 mA constant current excitation

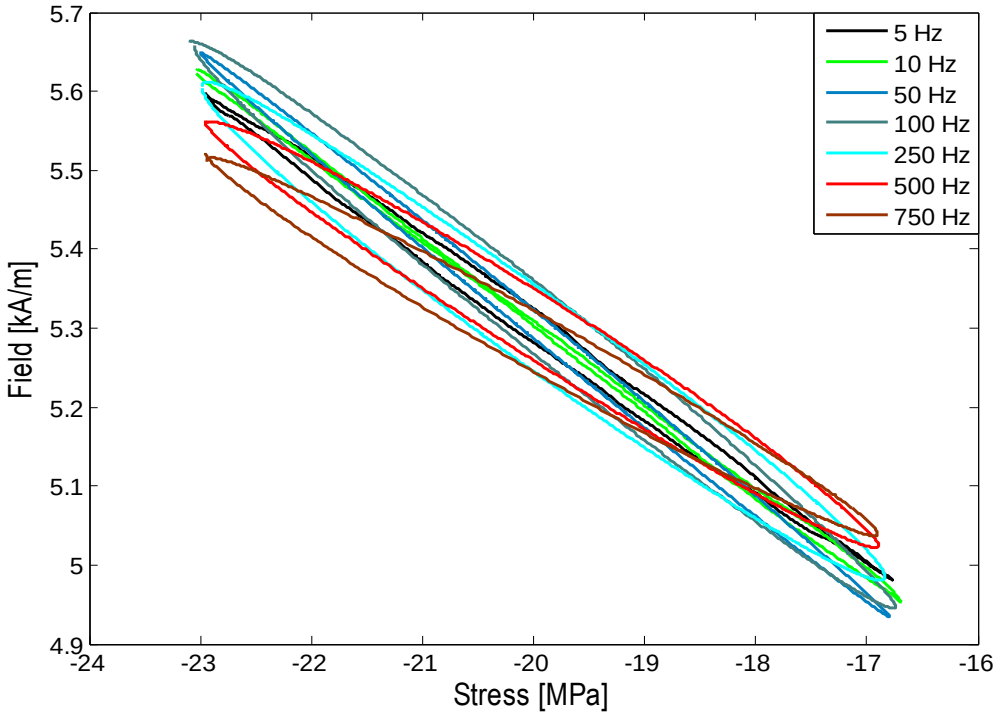

Figure 3.9: Field versus stress for seven frequencies (5, 10, 50, 100, 250, 500, 750 Hz) with 500 mA constant current excitation

3.4 Analysis and Discussion

From the results it can be seen that the hysteresis, elastic modulus, and sensitivity varies at different frequencies of the stress signal. The slope of the flux density versus stress loop indicates the sensitivity of Galfenol. The slope was estimated by using a first order polynomial to fit a straight line to the entire loop. Figure 3.10 shows the sensitivity as a function of the stress excitation frequency. In general, the sensitivity decreases as the input frequency increases, and the decrease becomes rapid for frequencies above 100 Hz. It can be concluded from the figure that low stress input frequencies are desirable for Galfenol based sensors to operate.

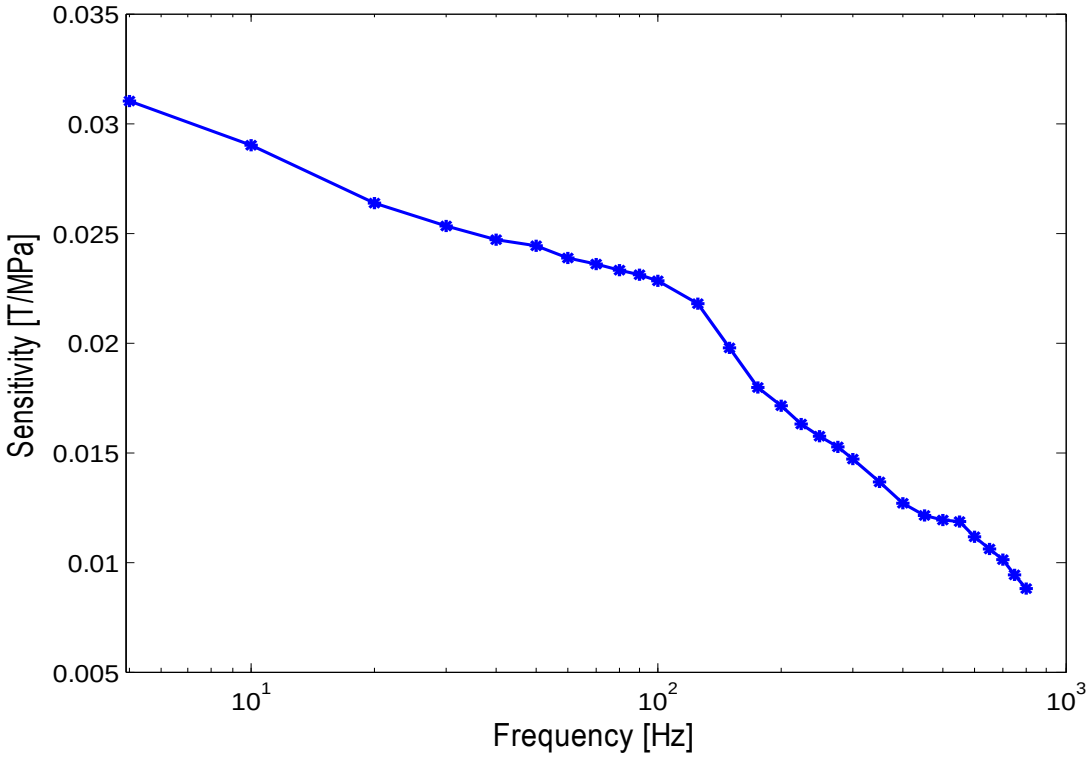

Figure 3.10 (a): Sensitivity versus frequency of input stress signal

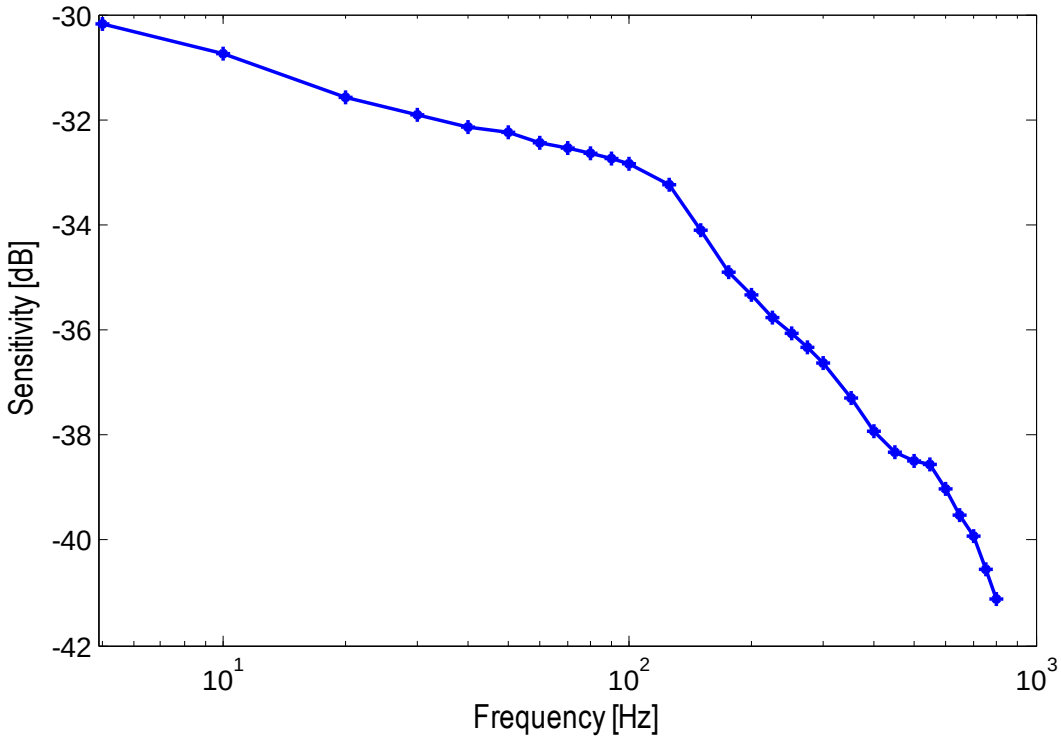

Figure 3.10 (b): Sensitivity (dB scale) versus frequency of input stress signal

Figure 3.11 shows how elastic modulus changes with varying frequencies of actuation. Elastic modulus is the ratio of stress to strain. Similar to the sensitivity calculation, the modulus was also calculated by fitting a linear line to the loop. From the figure there is no much change in modulus with the frequencies from 5 Hz to 200 Hz. With the stress input frequencies above 500 Hz, the elastic modulus increases rapidly, up to 68 GPa at 800 Hz. Figure 3.12 depicts the Delta-E effect as a function of the frequency of the input stress signal. The Delta-E effect is defined as the Young's modulus at magnetic saturation minus Young's modulus at the magnetic unsaturated state divided by the Young's modulus at the magnetic unsaturated state.

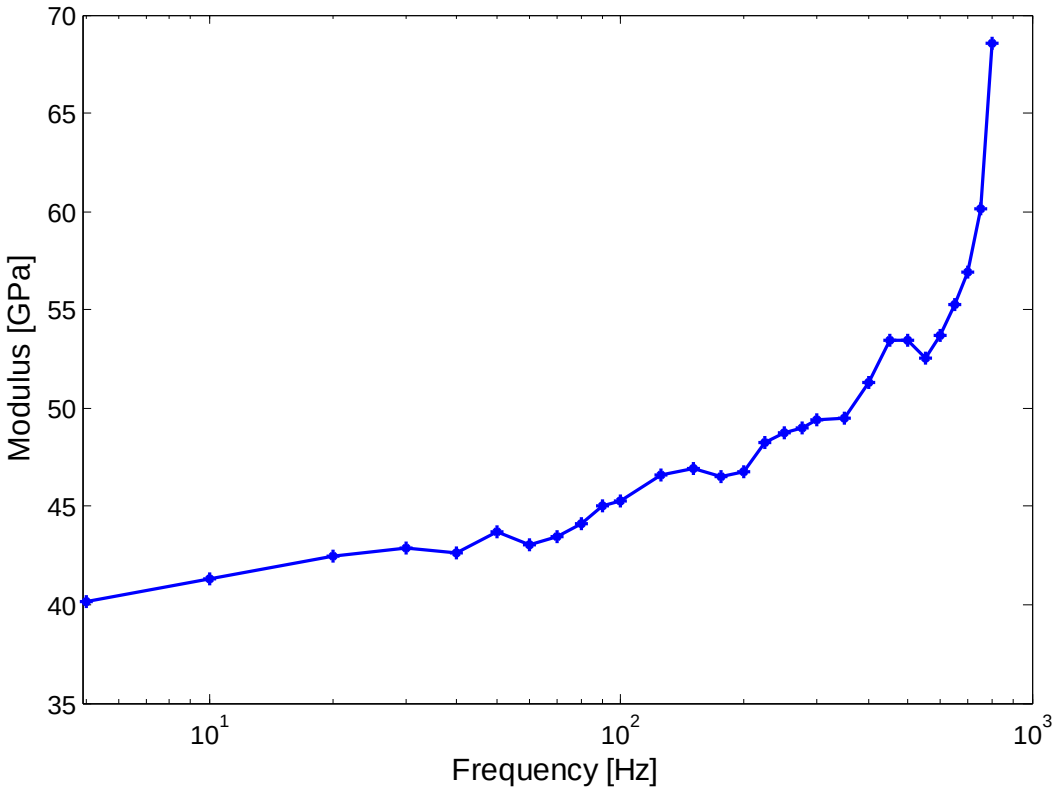

Figure 3.11: Elastic modulus versus frequency of input stress signal

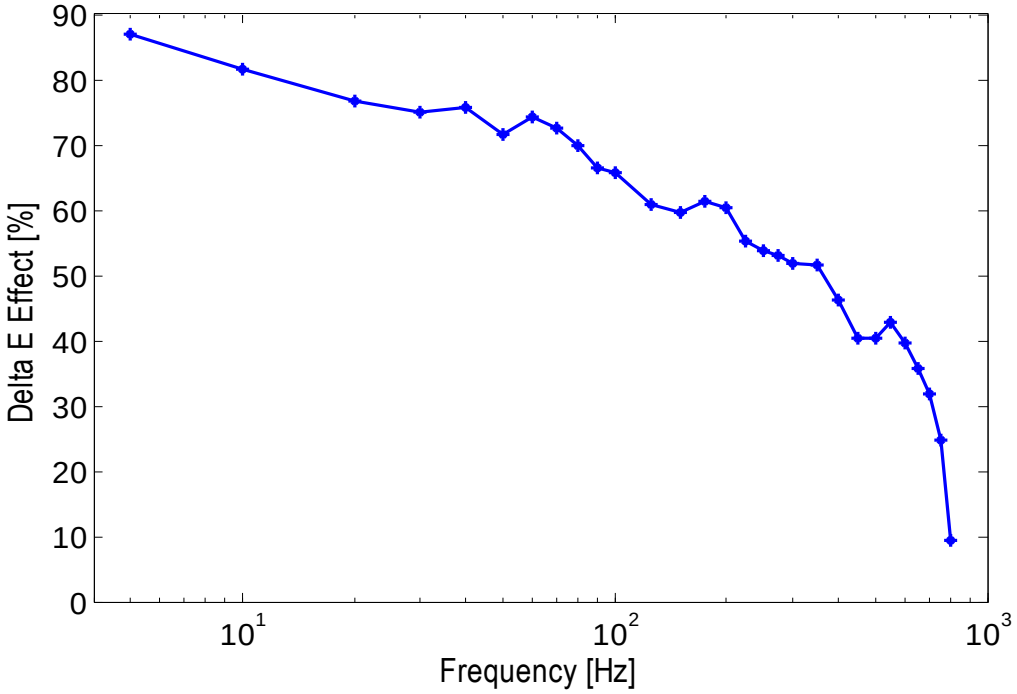

Figure 3.12: Delta-E Effect versus frequency of input stress signal

The hysteresis as a function of frequency of the input stress signal is shown in Figure 3.13 (stress - flux density), Figure 3.14 (stress - strain), and Figure 3.15 (stress - field). The area of the minor loop indicates the hysteresis, which was calculated through numerical integration method. The minor loop was first divided into two curves: one curve for the compression process, and one for release of the compressive force. The numerical integration for each curve was calculated, and then the hysteresis loss was obtained from the difference of the two numerical integrations. From the figures it is clear that there is not much change in hysteresis for the stress input frequencies between 5 Hz to 100 Hz. Therefore, in order to reduce the hysteresis loss, it is desirable for Galfenol based sensors to operate between 5 Hz to 100 Hz.

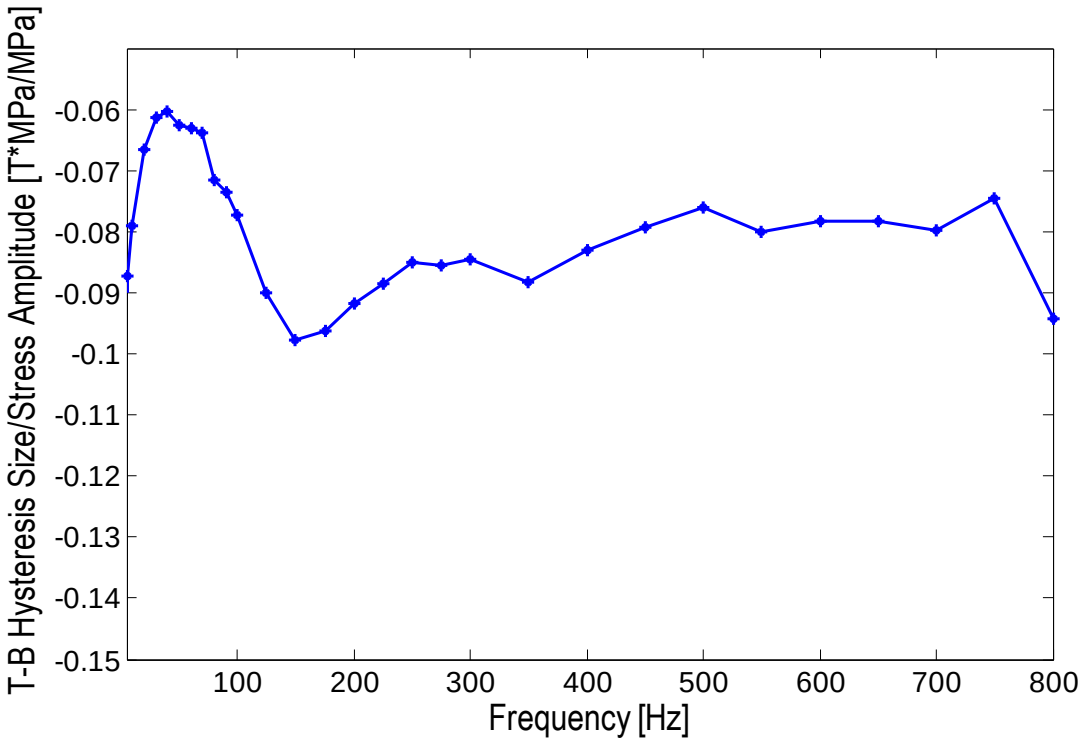

Figure 3.13: Stress-flux density hysteresis versus frequency of the input stress signal

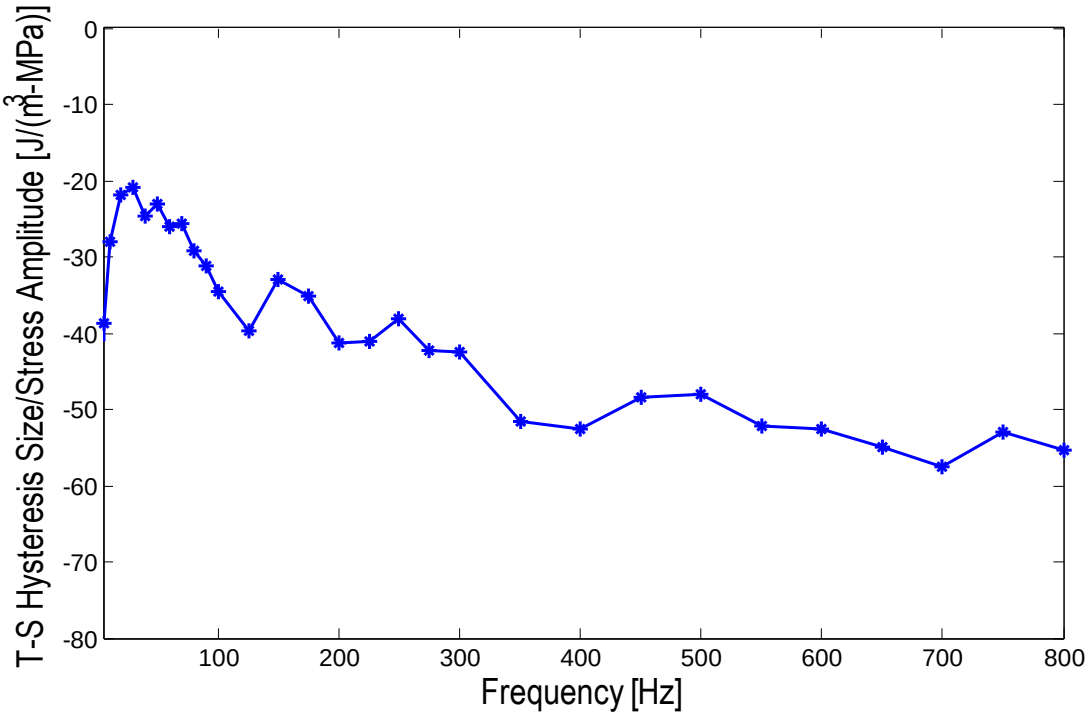

Figure 3.14: Stress-strain hysteresis versus frequency of the input stress signal

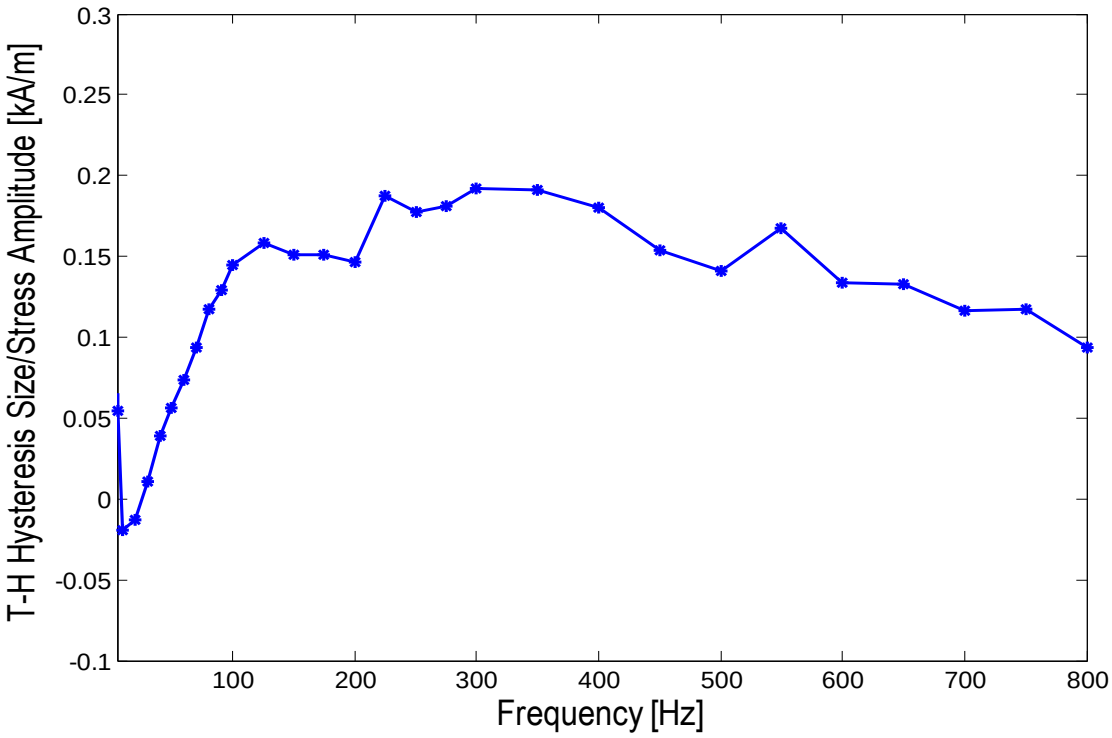

Figure 3.15: Stress-field hysteresis versus frequency of the input stress signal

CHAPTER 4

ROLLED GALFENOL SHEETS AND GALFENOL ENBEDDING

4.1 Rolled Galfenol Sheets

Currently, rolled Galfenol sheets are likely to be the most economical method of manufacturing. They are ideal for incorporating into active structural members, such as unimorph or bimorph beams for actuators or sensors [18]. The majority of the applications of Galfenol alloys, such as transducers and energy harvesters, requires lamination or production in thin sheet form. Galfenol alloys manufactured in sheets will eliminate the effect of its high magnetic permeability during high frequency operation, achieving a reduction of eddy current loss during device operation [19]. In addition, since Galfenol contains approximately eighty percent of iron, corrosion resistance is a critical issue in designs of Galfenol based sensors and actuators. This problem can be solved by embedding Galfenol into corrosion resistant members.

Bridgman Galfenol steel has a composition of 18.4 at.% gallium with 1002 low carbon steel addition, which can be used in force or torque sensing applications. Additions of carbon steel alloys could improve the mechanical strength of Galfenol alloys. At a condition of 7 ksi pre-load and 500 Oe magnetic field, the magnetostriction of the Galfenol steel is from 180 to 200 ppm [20]. Figure 4.1 is a highly textured polycrystalline 18.4 at.% gallium Galfenol sheet with 1002 low carbon steel addition. This Galfenol sample was obtained from Etrema Products Inc.

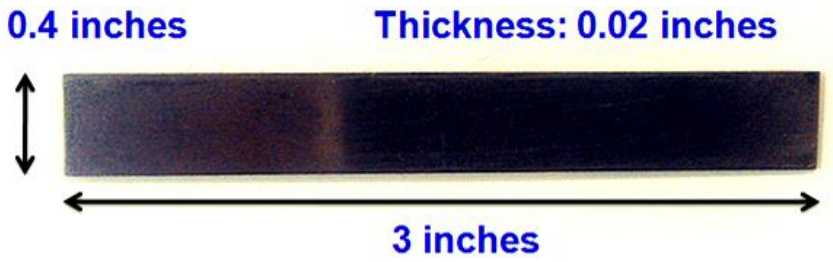

Figure 4.1: Rolled Galfenol steel ($Fe_{81.6}Ga_{18.4}$ plus 1002 steel additions)

A study of the magnetostriction behavior of the rolled Galfenol sheet ($Fe_{81.6}Ga_{18.4}$ plus 1002 steel additions) was conducted at quasi-static conditions. The tests were conducted at constant stress levels of 2 lb, 4 lb, 6 lb, 8 lb for tensile tests, and -12 lb to -2 lb in 2 lbs steps for compressive tests. A schematic image of the test setup for the measurements is shown in Figure 4.2. The actual test setup is shown in Figure 4.3. The magnetic circuit used in this measurement was obtained from Scheidler [21]. The experimental results of the magnetostriction measurements are shown in Figure 4.4 and 4.5. The saturation strain at each stress level was lower than we expected, which may caused by the oxidation layer on

the surface of the sample. Also, because of the thin sheet geometry, bending may also lead to a reduction in strain measurement. The results need to be further validated.

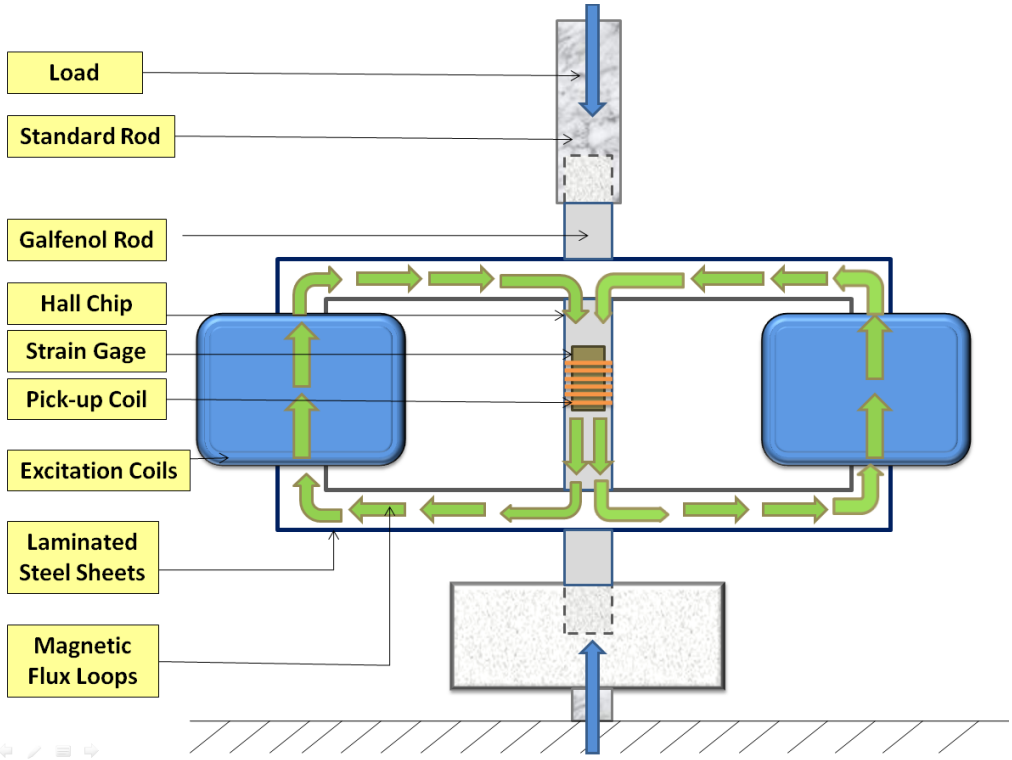

Figure 4.2: Schematic of test setup for quasi-static characterization of rolled Galfenol steel

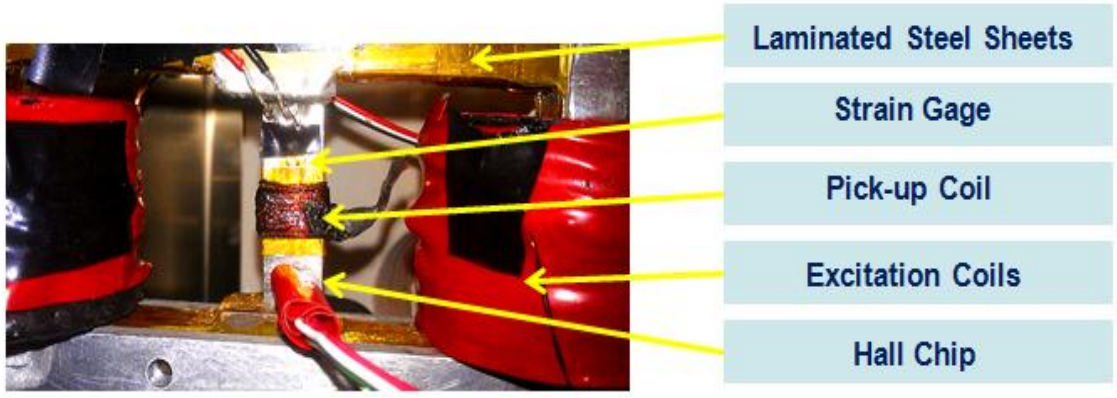

Figure 4.3: Test setup for quasi-static characterization of rolled Galfenol steel

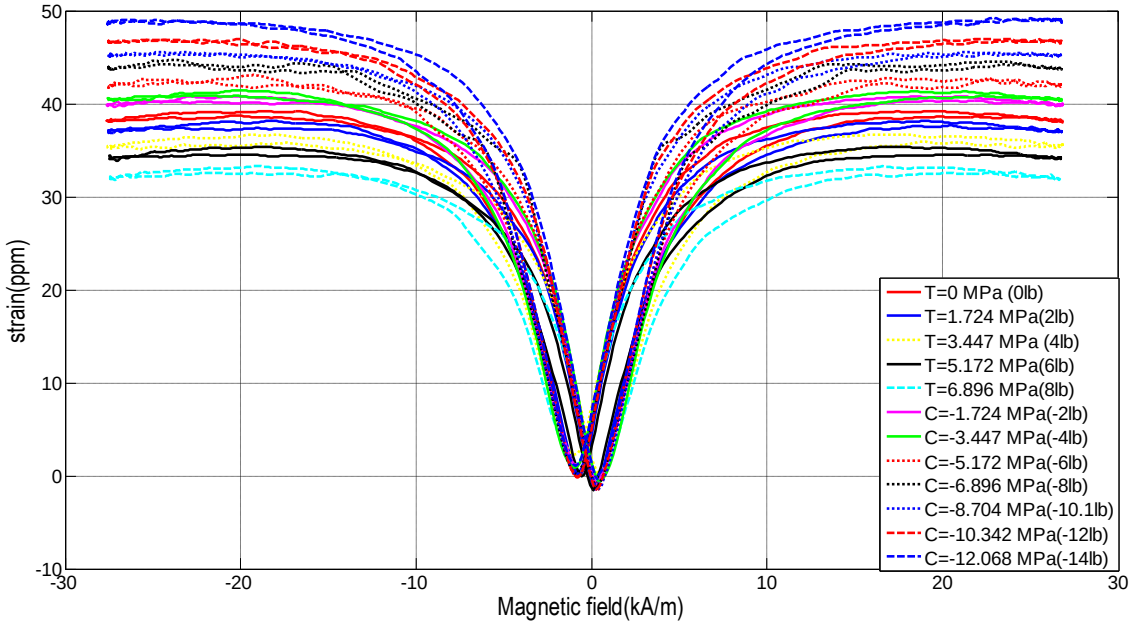

Figure 4.4: Strain versus field for rolled Galfenol steel sheet

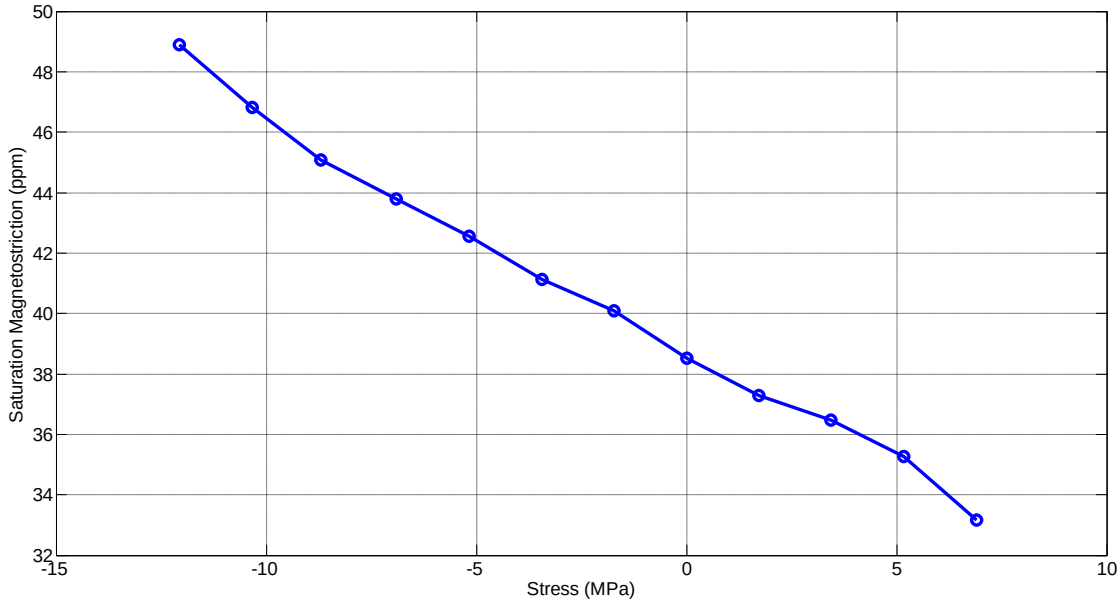

Figure 4.5: Saturation magnetosriction versus stress for rolled Galfenol steel sheet

4.2 Galfenol Embedding

4.2.1 Ultrasonic Additive Manufacturing (UAM)

Ultrasonic Additive Manufacturing is a welding process that builds up solid metal objects through ultrasonically welding successive layers of metal tape into a three-dimensional shape. This welding process was introduced by Solidica in 2000, which is promising in a wide range of applications, such as rapid prototyping, direct parts manufacture, and embedded smart materials [22]. A schematic of the welding process is shown in Figure 4.6. The ultrasonic vibrations are delivered by a transducer. The vibrations transmitted to a disk-shaped welding horn rolling in the x-axis, which creates a solid-state weld between the thin metal tape and the base plate. Spontaneous metal to metal bonding would then occur between the metal tape and the base plate [23].

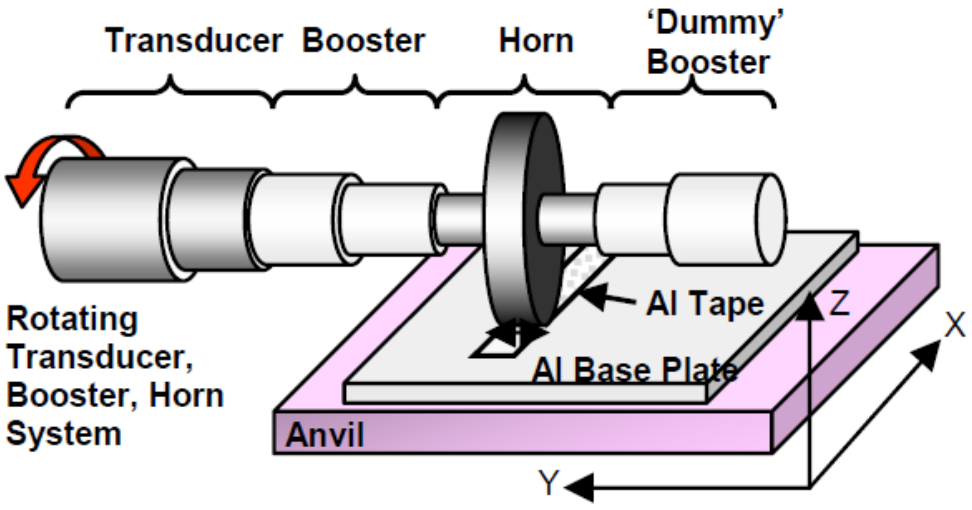

Figure 4.6: Schematic of UAM process [22]

4.2.2 Magnetostrictive Metal-Matrix Composite

In Galfenol-based sensors or energy harvesters, Galfenol sheets are often incorporated into other structures to create active composites. Compared to traditional welding methods, UAM provides unprecedented opportunities to develop seamless Galfenol embedded composites without degrading the properties of the Galfenol sheets [23]. For a composite to function, sufficient coupling between the bulk deformation and Galfenol deformation need to be achieved to maximum the mechanical response as well as the magnetic response [21]. A Galfenol-aluminum composite was made by Scheidler [21] using UAM for a study of the behavior of the active composite as well as the coupling between Galfenol and substrate. The rolled Galfenol steel-aluminum composite is shown in Figure 4.7. The actuation behavior of the composite was characterized and the experimental results can be seen in Figure 4.8 and 4.9.

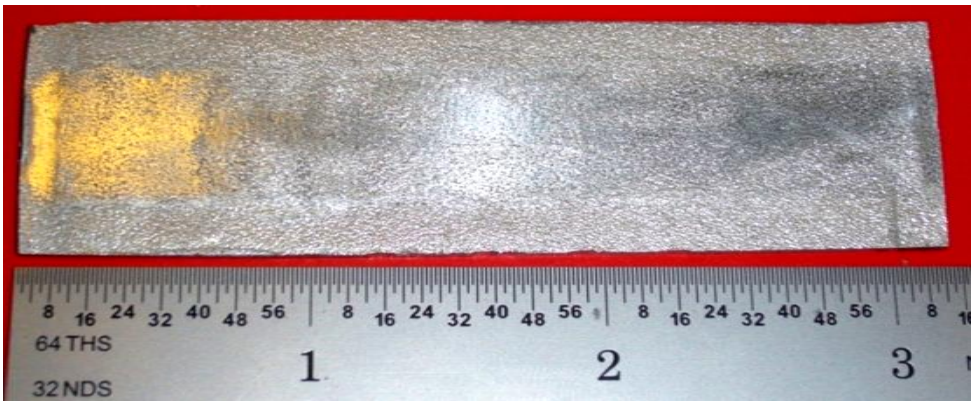

Figure 4.7: Rolled Galfenol steel – aluminum composite [24]

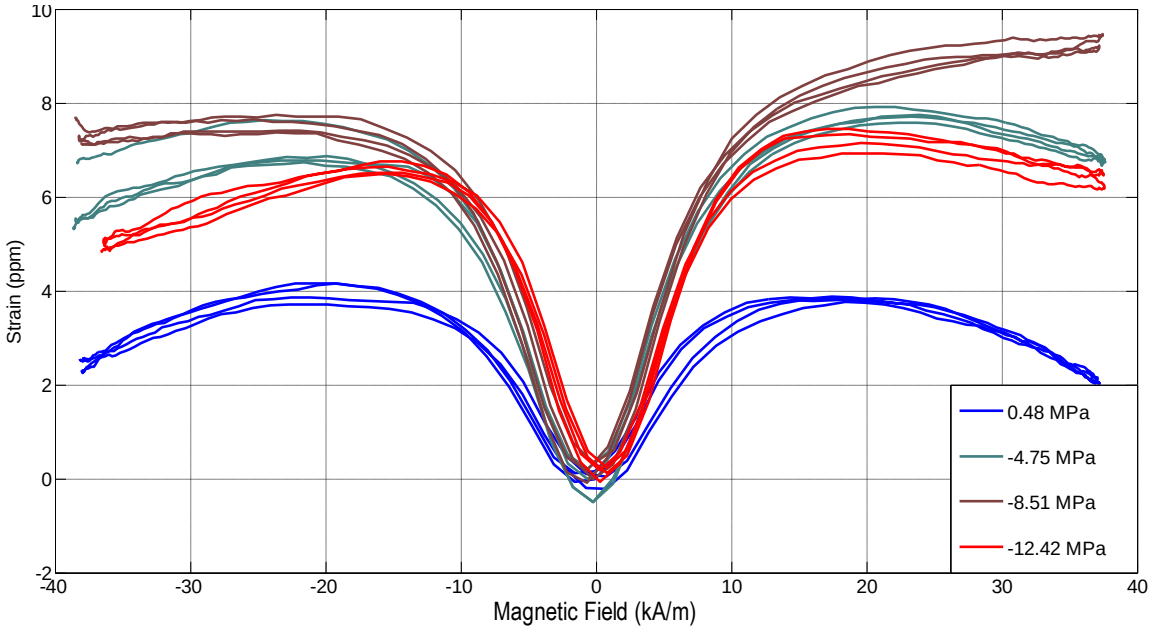

Figure 4.8: Strain versus field for rolled Galfenol steel – aluminum composite; Bias stress (0.48, -4.75, -8.51, -12.42 MPa)

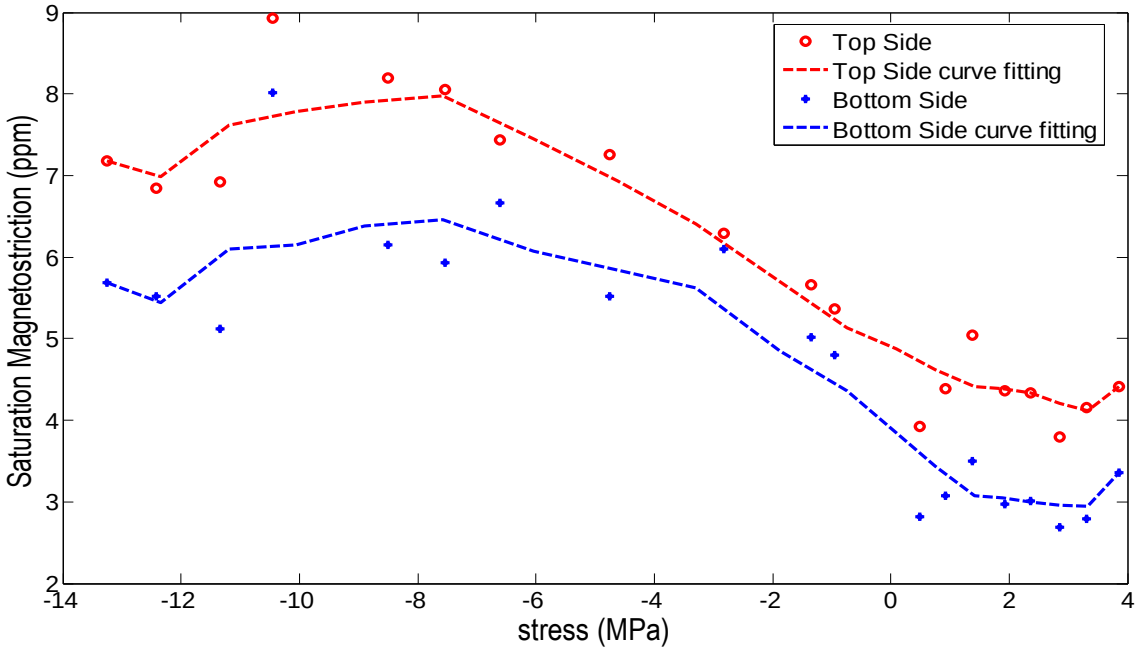

Figure 4.9: Saturation magnetostriction versus stress for rolled Galfenol steel – aluminum composite

CHAPTER 5

SUMMARY AND CONCLUSION

In this research, a highly textured, <100> oriented polycrystalline 18.4 at.% gallium Galfenol sample has been conducted and analyzed, with special interest in the sensing behavior. The testing apparatus was modified and improved based on a test-setup constructed by Walker [25]. Characterization of the Galfenol sample was conducted under both quasi-static and dynamic testing conditions. In the quasi-static characterization, both actuation and sensing behavior was characterized through major and minor loop testing. In the dynamic characterization, the sensing response was characterized through minor loop testing. The magnetic and mechanical responses of the material were observed and analyzed over a range of stresses and applied magnetic fields. These responses give a better understanding of the nonlinear and hysteretic behavior of Galfenol alloys. In addition, the results were used to optimize a constitutive model developed by Evans and Dapino [15], which will allow for more accurate designs of Galfenol-based actuators and sensors in applications.

Future work may include dynamic characterization of Galfenol at various fields or bias stress points. Also, dynamic characterization under different constant magnetic fields could be a great advancement in the knowledge of the nonlinearity and hysteresis of Galfenol.

These works would help gain a comprehensive set of experimental data to optimize the Galfenol model, which will aid in creating guidelines for determining the optimal conditions of Galfenol in various applications.

BIBLIOGRAPHY

[1] M. J. Dapino, R. Smith, F. Calkins, and A. Flatau. A magnetoelastic model for villari-effect magnetostrictive sensors. Technical report, 2002.

[2] F. Calkins, A. Flatau, and M. J. Dapino. Overview of magnetostrictive sensor technology. Journal of Intelligent Material Systems and Structures, 2007.

[3] M. J. Dapino, F. Calkins, and A. Faltau. Magnetostrictive devices. In John G. Webster, editor, Wiley Encyclopedia of Electrical and Electronics Engineering, pages 278-305. John Wiley & Sons, Inc., New York, NY, 1999.

[4] R. A. Kellogg. Development and modeling of iron-gallium alloys. Ph.D. thesis, Iowa State University, 2003.

[5] N.W. Hagood IV and M. J. Atalla. *Adaptive Structures and Technology*, Ninth International Conference, 1999.

[6] M. J. Dapino. On magnetostrictive materials and their use in adaptive structures. *Structural Engineering and Mechanics*, pages 303-329, 2004.

[7] J. Slaughter, E. Summers, Designing with Galfenol, ETREMA Products Inc. Ames, Iowa, 2013.

[8] S. Datta, M. Huang, J. Raim, T. Logasso, and A. Flatau. Effect of thermal history and gallium content on magneto-mechanical properties of iron-gallium alloys. *Materials Science and Engineering*, volume 435-436, pages 221-227, 2006.

[9] M. J. Dapino. Nonlinear and hysteretic magnetomechanical model for magnetostrictive transducers. Ph.D. thesis, Iowa State University, 1999.

[10] A. G. Olabi and A. Grunwald, Design and Application of Magnetostrictive "MS" Materials, 2006.

[11] G. Engdahl. *Handbook of Giant Magnetostrictive Materials*. Academic Pr, 2000.

[12] A.E. Clark, K.B. Hathaway, M. Wun-Fogle, J.B. Restorff, T.A. Lograsso, V.M.

Keppens, G. Petculescu, and R.A. Taylor. Extraordinary magnetoelasticity and lattice softening in bcc fe-ga alloys. *Journal of applied physics*, 93(10):8621-8623, 2003.

[13] E. Summers, T. Lograsso, and M. Wun-Fogle. Magnetostriction of binary and ternary fe-ga alloys. *Journal of Materials Science*, 42(23):9582-9594, 2007.

[14] R. Kellogg, A. Flatau, A. Clark, M. Wun-Fogle, and T. Lograsso. Temperature and stress dependencies of the magnetic and magnetostrictive properties of fe0.81ga0.19. *Journal of applied physics*, 91(10):7821-7823, 2002.

[15] P. Evans and M. Dapino. Efficient magnetic hysteresis model for field and stress application in magnetostrictive galfenol. *Journal of Applied Physics*, 107(6):063906 063906, 2010.

[16] C. Poeppelman. Characterization of magnetostrictive iron-gallium alloys under dynamic conditions. Undergraduate honors thesis, The Ohio State University, 2010.

[17] PCB Piezotronics Inc., Model. SN 22276 - 208C02 load cell.

[18] C. Mudivarthi, S. Datta, J. Atulasimha, and A. B. Flatau. A bidirectionally coupled magnetoelastic model and its validation using a galfenol unimorph sensor. *Smart Materials and Structures*, 2008.

[19] M. Brooks, E. Summers, and T.A. Lograsso. Gallium Content Effects in Low Carbon Steels. *Materials Science & Technology 2009 Conference and Exhibition*, Page 1442-1453, 2009.

[20] A. Mahadevan. Force and torque sensing with galfenol alloys. Master's thesis, The Ohio State University, 2009.

[21] J. J. Scheidler. Magnetostrictive metal-matrix composites. Undergraduate honor thesis, The Ohio State University, 2011.

[22] K. F. Graff, M. Short, and M. Norfolk. Very High Power Ultrasonic Additive Manufacturing (VHP UAM) for Advanced Materials. Edison Welding Institute, 2010.

[23] R. Hahnlen and M.J. Dapino. Active metal-matrix composites with embedded smart materials by ultrasonic additive manufacturing. In SPIE *Proceedings*, volume 7645, 2010.

[24] Courtesy by J.J. Scheidler, 2012.

[25] T. W. Walker. Experimental characterization and modeling of Galfenol (FeGa) alloys for sensing. Master's thesis, The Ohio State University, 2012.

APPENDIX

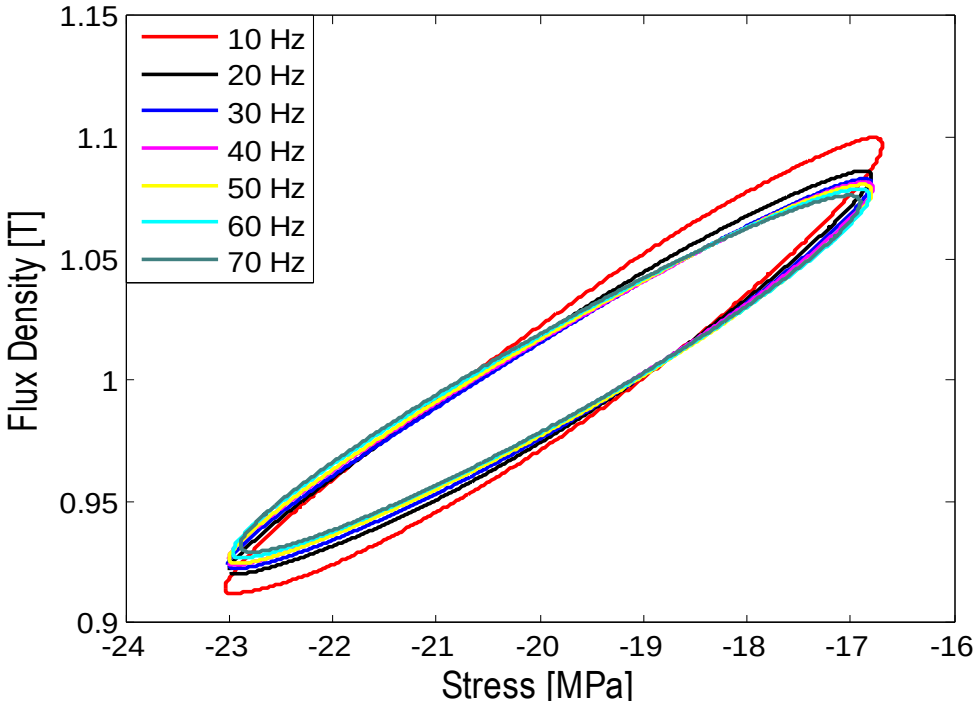

Figure A.1: Flux density versus stress for seven frequencies (10, 20, 30, 40, 50, 60, 70 Hz) with 500 mA constant current excitation; Bias stress: -19.85 MPa; Stress amplitude: 3MPa

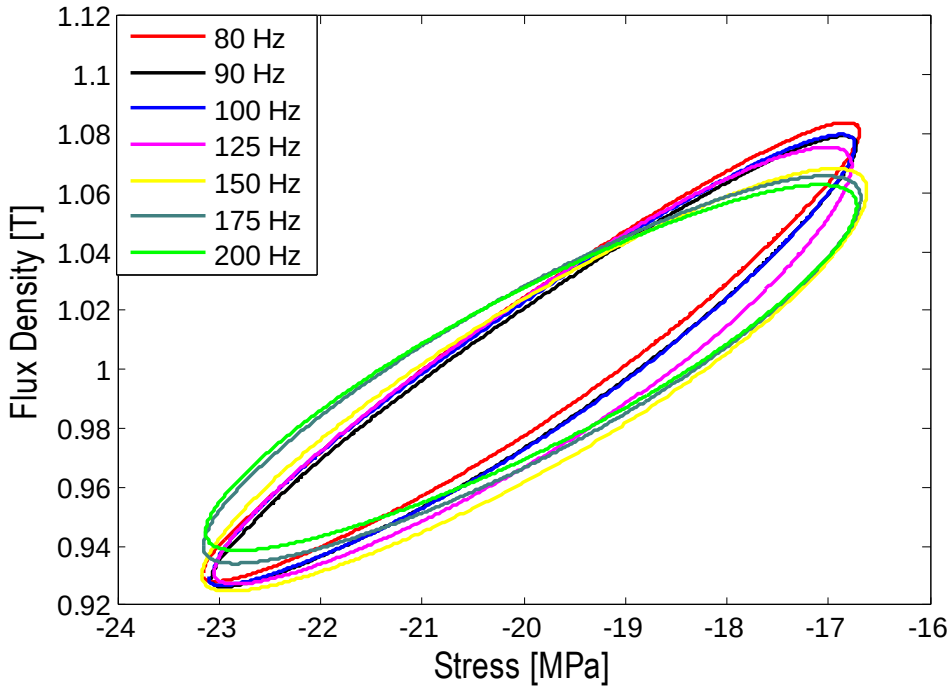

Figure A.2: Flux density versus stress for seven frequencies (80, 90, 100, 125, 150, 175, 200 Hz) with 500 mA constant current excitation; Bias stress: -19.85 MPa; Stress amplitude: 3MPa

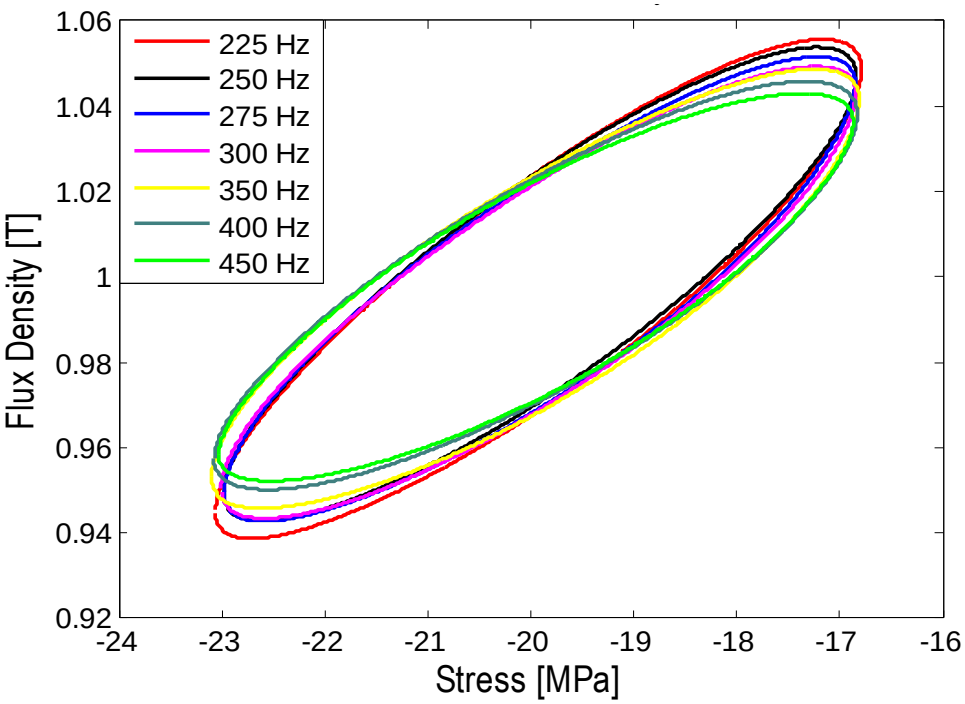

Figure A.3: Flux density versus stress for seven frequencies (225, 250, 275, 300, 350, 400, 450 Hz) with 500 mA constant current excitation; Bias stress: -19.85 MPa; Stress amplitude: 3MPa

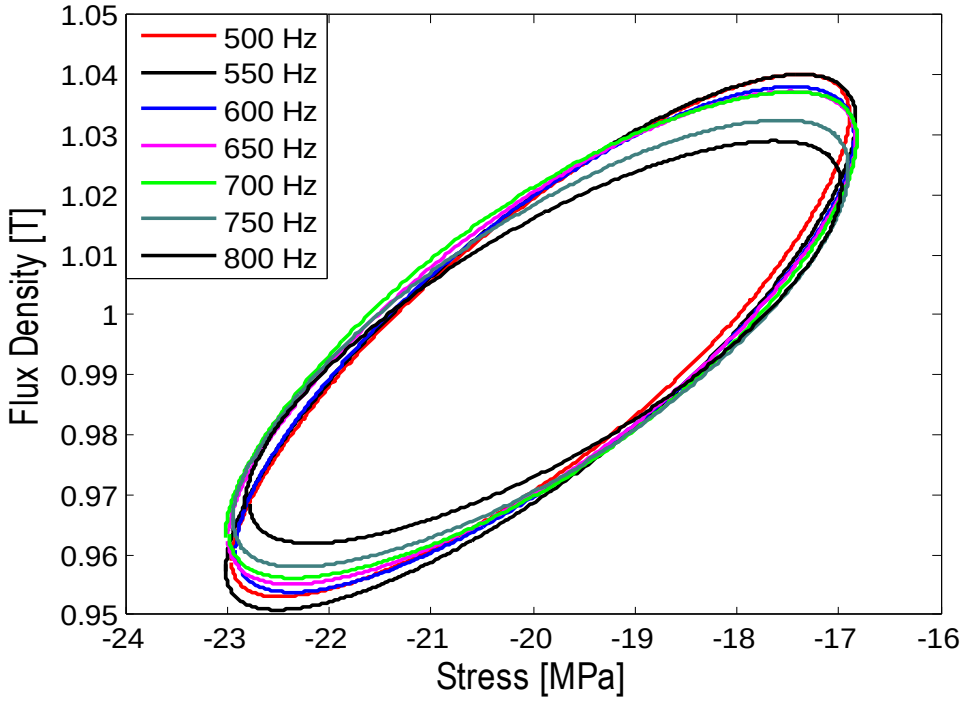

Figure A.4: Flux density versus stress for seven frequencies (500, 550, 600, 650, 700, 750, 800 Hz) with 500 mA constant current excitation; Bias stress: -19.85 MPa; Stress amplitude: 3MPa

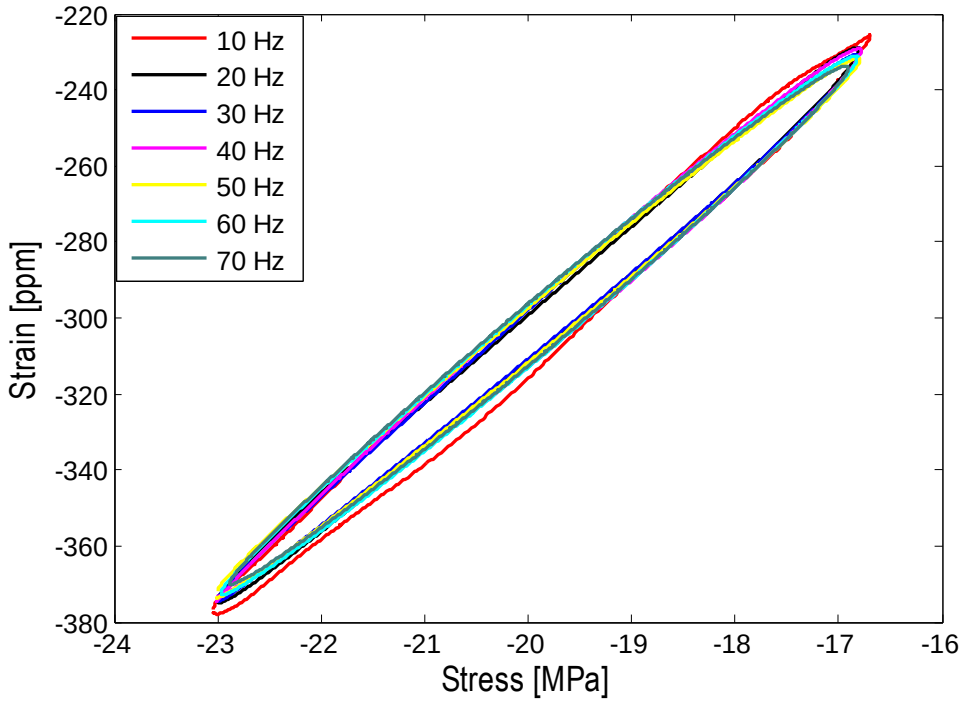

Figure A.5: Strain versus stress for seven frequencies (10, 20, 30, 40, 50, 60, 70 Hz) with 500 mA constant current excitation; Bias stress: -19.85 MPa; Stress amplitude: 3MPa

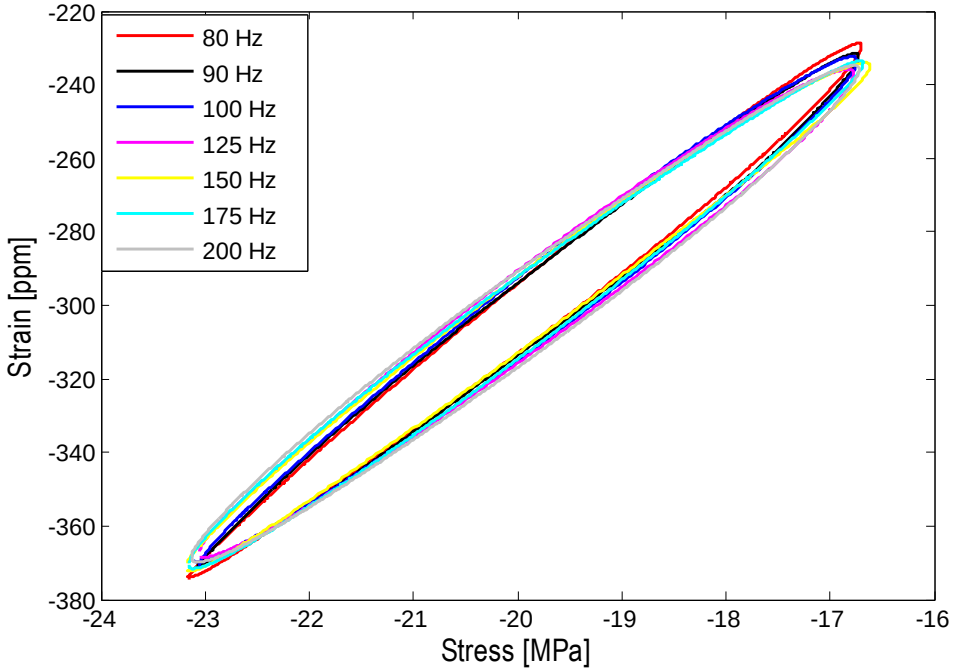

Figure A.6: Strain versus stress for seven frequencies (80, 90, 100, 125, 150, 175, 200 Hz) with 500 mA constant current excitation; Bias stress: -19.85 MPa; Stress amplitude: 3MPa

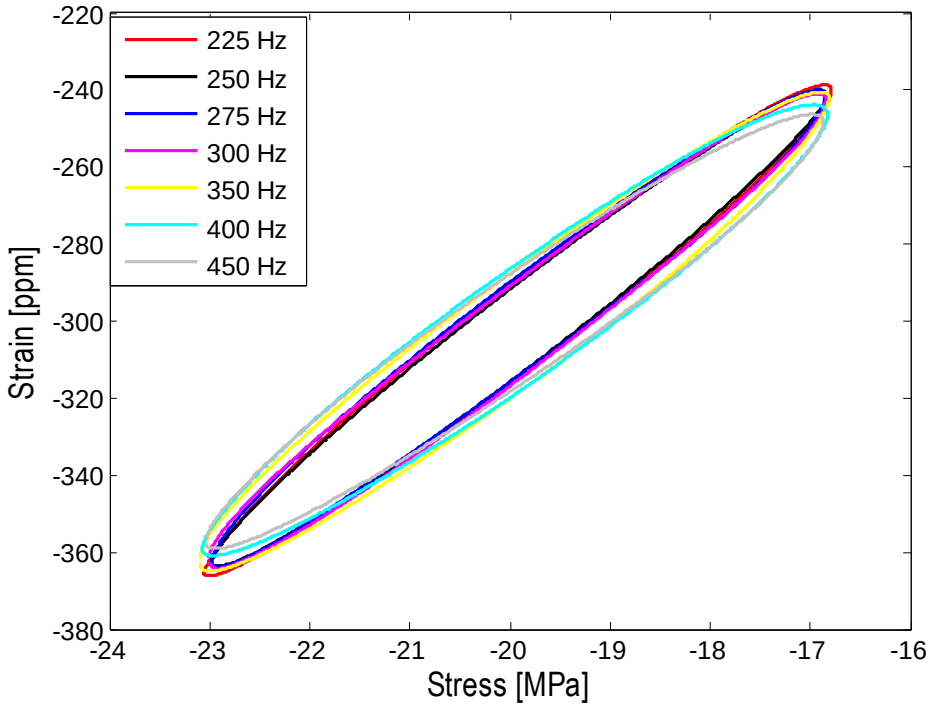

Figure A.7: Strain versus stress for seven frequencies (225, 250, 275, 300, 350, 400, 450 Hz) with 500 mA constant current excitation; Bias stress: -19.85 MPa; Stress amplitude: 3MPa

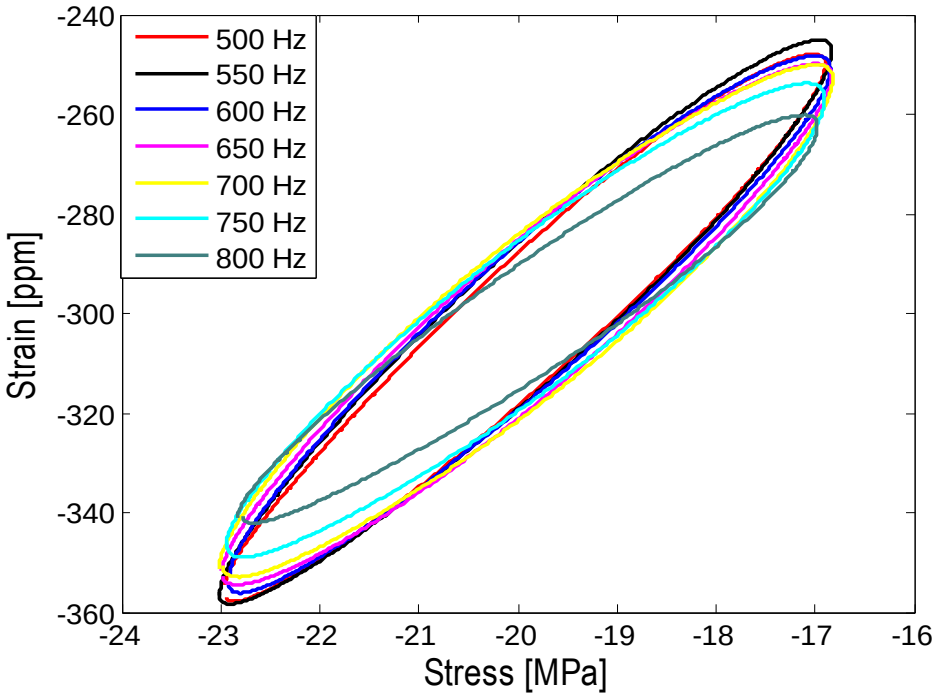

Figure A.8: Strain versus stress for seven frequencies (500, 550, 600, 650, 700, 750, 800 Hz) with 500 mA constant current excitation; Bias stress: -19.85 MPa; Stress amplitude: 3MPa

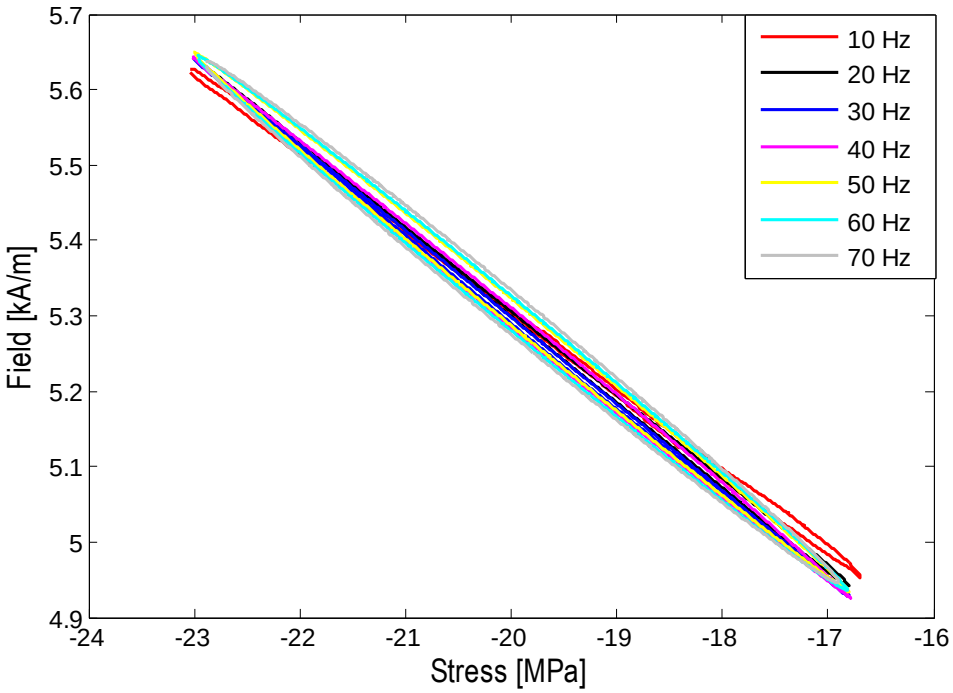

Figure A.9: Field versus stress for seven frequencies (10, 20, 30, 40, 50, 60, 70 Hz) with 500 mA constant current excitation; Bias stress: -19.85 MPa; Stress amplitude: 3MPa

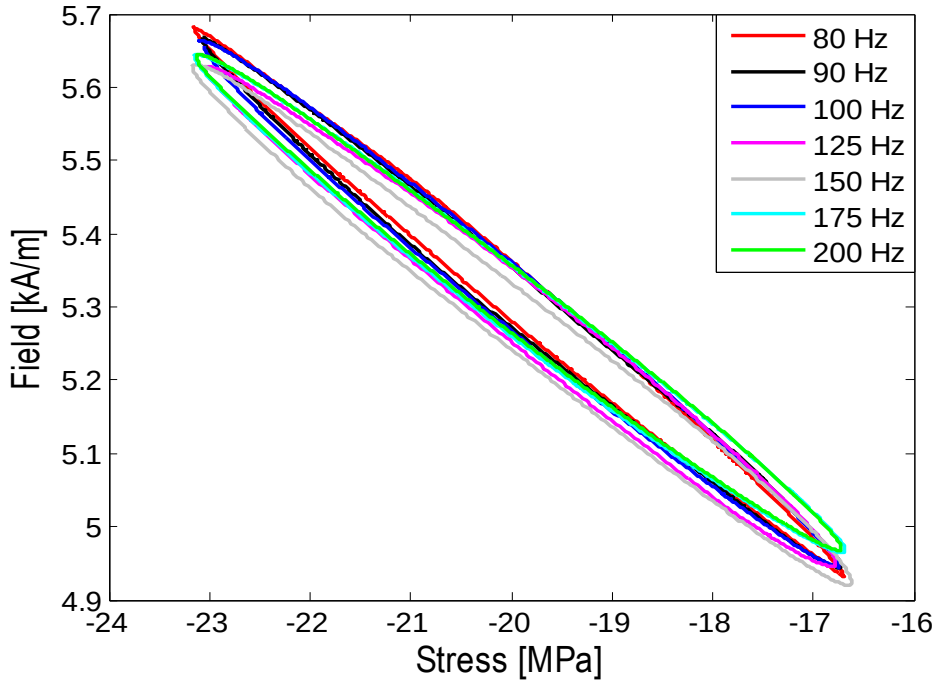

Figure A.10: Field versus stress for seven frequencies (80, 90, 100, 125, 150, 175, 200 Hz) with 500 mA constant current excitation; Bias stress: -19.85 MPa; Stress amplitude: 3MPa

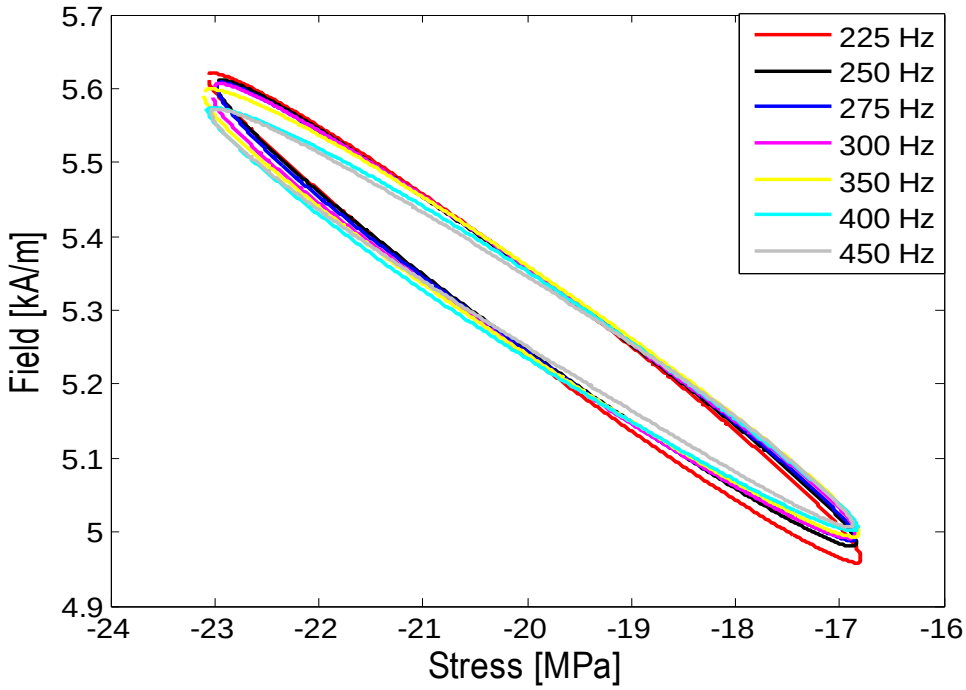

Figure A.11: Field versus stress for seven frequencies (225, 250, 275, 300, 350, 400, 450 Hz) with 500 mA constant current excitation; Bias stress: -19.85 MPa; Stress amplitude: 3MPa

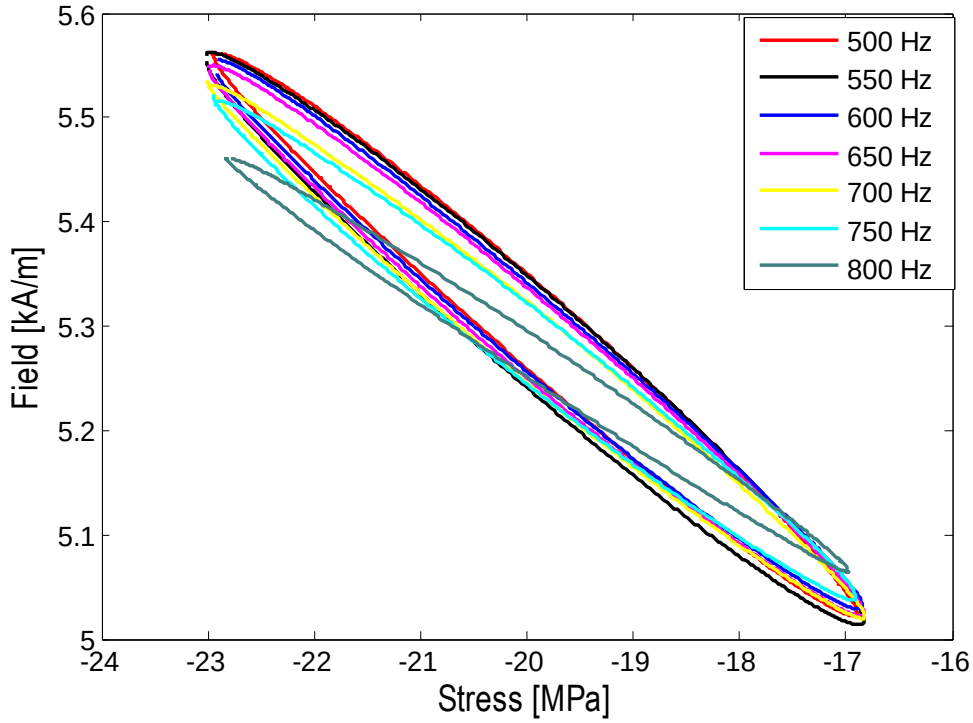

Figure A.12: Field versus stress for seven frequencies (500, 550, 600, 650, 700, 750, 800 Hz) with 500 mA constant current excitation; Bias stress: -19.85 MPa; Stress amplitude: 3MPa

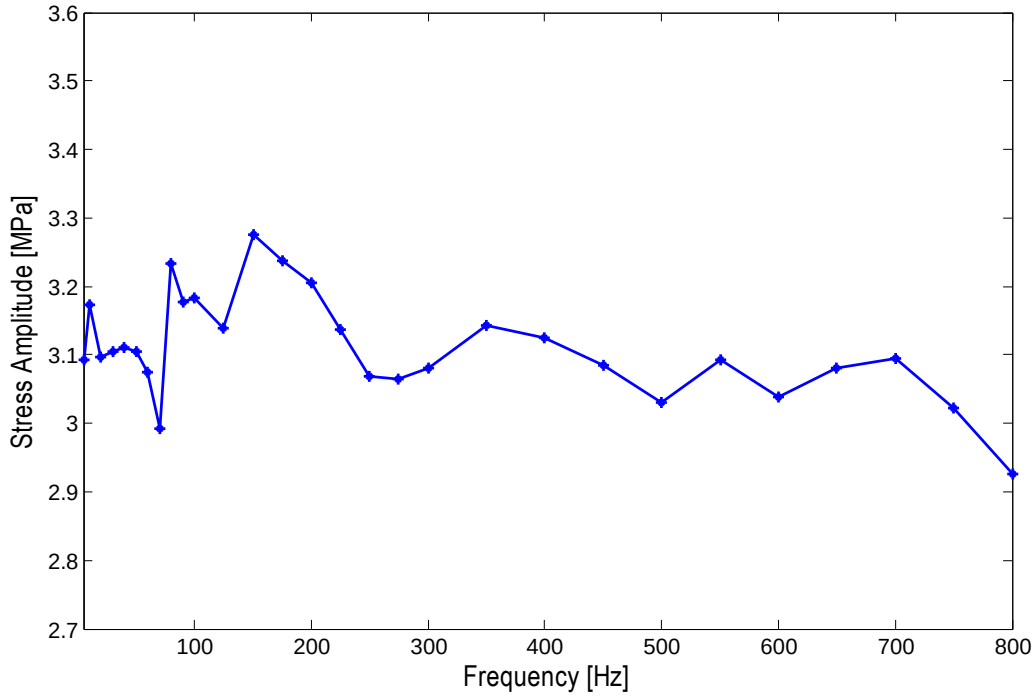

Figure A.13: Stress amplitude versus frequency for dynamic characterization